RMetS
Royal Meteorological Society

Observations of dual slantwise circulations above a cool undercurrent in a mesoscale convective system

K. A. Browning,[a]*J. H. Marsham,[b] J. C. Nicol,[c] F. M. Perry,[b] B. A. White,[a] A. M. Blyth[b] and S. D. Mobbs[b]

[a]*University of Leeds, UK*
[b]*National Centre for Atmospheric Sciences (NCAS), University of Leeds, UK*
[c]*NCAS, University of Reading, UK*
*Correspondence to: K. A. Browning, High Croft, Under Loughrigg, Ambleside, Cumbria, LA22 9LJ, UK.
E-mail: jmarsham@env.leeds.ac.uk

A series of mesoscale convective systems (MCSs) was observed in the UK during one of the Intensive Observation Periods (IOP 3) in the Convective Storm Initiation Project (CSIP). A detailed case-study of one of the MCSs, involving some novel interpretation of single Doppler radar data, reveals the evolution of stacked slantwise circulations associated with elevated upright convection. A feature of this occasion was the existence near the surface of a strong undercurrent of cool air flowing against the direction of travel of the storm. The air feeding both the upright and slantwise ascent originated not from near the surface but, rather, from layers between 1 and 3 km. The upright convection was intense at first and was accompanied by a region of dry subsidence surrounding it, together with the alternating layers of slantwise ascent and descent within the storm's precipitation area. When the elevated upright convection weakened, vigorous slantwise motions continued for some time, but their slope decreased from the initial 1 in 4 to 1 in 9. The lowermost layer of slantwise descent corresponded to a moderately intense rear-inflow jet. The rear-inflow jet did not penetrate the cool undercurrent and reach the surface; instead, beneath where it impacted the warm air capping the undercurrent, the undercurrent took on the structure of a gravity wave without stagnation. The raised head of the undercurrent lifted overlying air of high wet-bulb potential temperature sufficiently to overcome the convective inhibition. **Copyright © 2010 Royal Meteorological Society**

Key Words: MCS; slantwise convection; rear-inflow jet; atmospheric bore; CSIP; Doppler radar

Received 17 March 2009; Revised 19 August 2009; Accepted 9 December 2009; Published online in Wiley InterScience 12 February 2010

Citation: Browning KA, Marsham JH, Nicol JC, Perry FM, White BA, Blyth AM, Mobbs SD. 2010. Observations of dual slantwise circulations above a cool undercurrent in a mesoscale convective system. *Q. J. R. Meteorol. Soc.* **136**: 354–373. DOI:10.1002/qj.582

1. Introduction

A mesoscale convective system (MCS) is a cloud system that occurs in connection with an ensemble of thunderstorms and produces a contiguous area of precipitation about 100 km or more in horizontal scale in at least one direction (Houze, 1993, 2004). MCSs tend to be distinct entities that owe their organization to some form of mesoscale dynamical process. The present paper presents observations of the structure and evolution of an MCS that contained a mixture of convective and stratiform precipitation, the latter being associated with trailing slantwise circulations as in the conceptual model of Houze *et al.* (1989). Their model shows that behind the main region of deep convection there

is a broader region of slantwise ascending front-to-rear flow in the middle troposphere situated above a similarly sloping layer of descending rear inflow. In the present case, however, there were two pairs of slantwise circulations. Such slantwise circulations are sometimes referred to as slantwise convection but to avoid confusion we shall reserve the use of the term convection here to ordinary 'upright' convection.

The present paper gives an analysis of a small MCS that was observed on the edge of a frontal zone in southern England during IOP 3 of the Convective Storm Initiation Project (CSIP; Browning *et al.*, 2007). The lowermost descending limb of the slantwise circulation observed in this study had a steep slope of 1 in 4 in the initial stages when the convection was vigorous. However, with time, as the convection in the MCS weakened, the slope of the slantwise descent decreased to about 1 in 9. Although the authors are not aware of such major changes in slope having been documented before, the slantwise descent corresponds to the rear-inflow jet that has been observed in many MCSs. In a study of 18 MCSs in the USA, Smull and Houze (1987) found that three were associated with strong rear inflow (relative flow $>$ $10\,\mathrm{m\,s^{-1}}$), five had moderate rear inflow ($5-10\,\mathrm{m\,s^{-1}}$) and the remainder had less than this. The rear inflow in the present study was in the moderate category. There is some uncertainty as to the extent to which such circulations are generated internally by the convective systems themselves, as hypothesized by Smull and Houze (1987), or are the manifestations of upstream variations in the pre-convective environment. Observations by Klimowski (1994) support the idea that the rear inflow systematically develops within the MCS. Lafore and Moncrieff (1989) have shown how a rear-inflow jet can develop in response to the developing horizontal and vertical buoyancy gradients aloft. Pandya and Durran (1996) suggest that both the rear-inflow jet and the front-to-rear slantwise ascent are a gravity wave response to the mean heating in the convective region.

A key feature of the MCS in the present study is that the convection and slantwise circulations occurred above a statically stable layer that occupied the lowest kilometre or two adjacent to the ground. Since it also formed in a baroclinic zone, it evidently corresponded to what Fritsch and Forbes (2001), in their review, refer to as a Type-1 event. Analyses of such events have revealed that the moist downdraughts sometimes do not penetrate to the surface through the large-scale low-level layer of cool air, e.g. Browning and Hill (1984) for a MCS in the UK, and Fortune *et al.* (1992), Smull and Augustine (1993) and Trier and Parsons (1993) for large MCSs (Mesoscale Convective Complexes) in the USA. This was true also in the present case. We shall show that, where the downward branch of the slantwise circulation impacted on the low-level stable layer, it was associated with a wave structure within the underlying cool air.

In some respects the wave structure in the present study resembles a bore. A bore is an example of a hydraulic jump in which there is a sudden increase in depth associated with a change in flow rate (Simpson, 1997). According to Johnson and Mapes (2001), bore-like disturbances often occur in connection with surface-based stable layers and may be generated by an impulsive forcing such as a downdraught impinging upon the stable layer. According to Knupp (2006), a bore produces a long-lasting pressure increment whereas in the present case-study the pressure rise was transient and so we shall refer to it in more general terms as a wave rather than a bore.

A unique feature of the present paper is that the observations clearly reveal the relationship of the wave feature to the lowermost descending slantwise flow (rear-inflow jet) where it impinged upon the stable layer. The nose of the rear-inflow jet remained closely coupled to the wave feature and so any forcing can be regarded as continuous rather than in the form of, effectively, a single impulse in which the wave or bore propagates away from the source, as found in many other studies (e.g. Wakimoto and Kingsmill, 1995; Kingsmill and Crook, 2003; Knupp, 2006).

An overview of the MCS is given in section 2 and a two-dimensional analysis of the detailed structure of the evolving MCS, including the elevated convection and slantwise circulations, is presented in section 3. The MCS was one of a number of similar systems that occurred on 24 June 2005, some of which produced significant localized flash floods, within the area covered by the CSIP observational facilities. The observational network for CSIP, centred on Chilbolton in southern England, is summarized in the review article by Browning *et al.* (2007). Key tools exploited in this study include the dual-polarization S-band Doppler radar at Chilbolton (Goddard *et al.*, 1994) whose 25 m dish provided high sensitivity and superior resolution (0.28 degree beamwidth). Also used were a lidar ceilometer, a network of automatic weather stations and ascents from three of the seven radiosonde sites within the CSIP area. Operationally available imagery was also used from the Meteosat Second Generation (MSG) satellite and from the UK Weather Radar Network. There have been many studies of slantwise circulations within MCSs using Doppler radar and other observations, and in some respects this is just one more such study; however, the novel aspect of the present study is the way in which several parameters from the Doppler data – including highly resolved vertical shear and spectral width as well as reflectivity – are used to reveal the details of the convection and slantwise flows and their interaction with the underlying cool air.

2. Overview of the MCS

2.1. *The evolving MCS in relation to the synoptic situation*

The synoptic situation at 1200 (all times in UTC) on 24 June 2005 is shown in the operational Met Office analysis in Figure 1. The CSIP area was under the influence of a shallow low situated just to the south, over the north coast of France. Figure 2 shows an analysis of the geopotential height of the 32 °C (305 K) dry-bulb potential temperature (theta) surface which, as we show later, was close to one of the layers that fed the convective updraughts. The arrows in Figure 2 show this air coming from the direction of northwest Spain. Although not evident in the operational frontal analysis in Figure 1, it is clear from Figure 2 that the CSIP area was within a baroclinic zone, with isentropic surfaces sloping upwards towards the west and north. Using ECMWF operational analyses, isentropic trajectories were run backwards from south of England (50°N, 3.5°W) at 1200 UTC on 24 June. These showed air with a potential temperature of 32 °C (305 K) originating from northwest Spain four days earlier and ascending at $1.5\,\mathrm{cm\,s^{-1}}$ for the preceding 24 h, i.e. there was an upslope component to

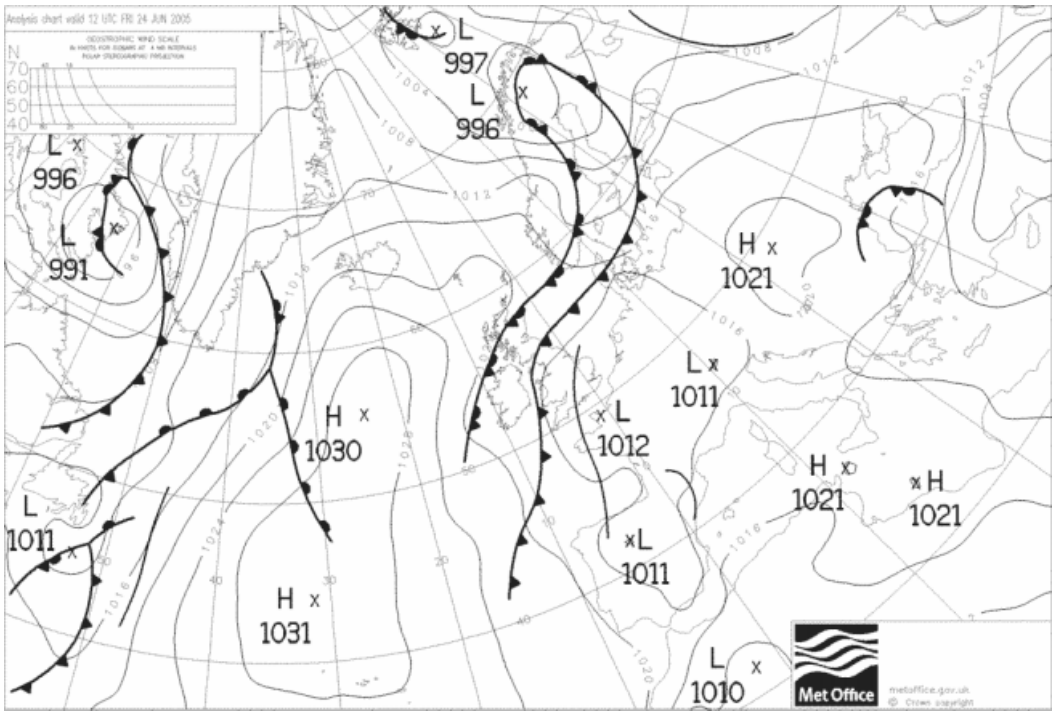

Figure 1. Met Office surface analysis for 1200 UTC, 24 June 2005. ©Crown Copyright 2005.

the isentropic flow, even though this is not immediately apparent from Figure 2.

Several MCSs occurred over southern England along what is marked as a trough line in Figure 1. Some of these are shown in the series of hourly satellite and radar-network images in Figure 3, where they are labelled B, C and D (MCS A affected the CSIP area much earlier, as shown later by Figure 5). The present study focuses on the MCS labelled C. A further MCS (unlabelled), just to the northwest of C, crossed part of the CSIP area but missed most of the automatic weather stations (plotted red on the satellite images). The first image, Figure 3(a), shows C as a new cumulonimbus cloud cell developing over the sea at 1045; the earliest evidence of deepening convection was between 1015 and 1030. Figure 3(c) shows C at 1145. It has a rapidly expanding anvil and there is a concentric ring of lower-level cloud at a distance of 10 km behind the anvil edge, with an intervening cloud-free zone, presumably due to dry subsidence in the immediate surroundings of the storm. (Radar evidence shown later reveals subsidence just ahead of the storm core as well). A convective cell can be seen in Figure 3(c) to have developed just outside the ring of subsidence, probably as a result of secondary initiation, on the storm's right rear flank. This developed and blended with the rest of MCS C, causing the core of the MCS to propagate approximately to the right (south) of the mid-level wind direction. The anvil of MCS C had expanded further by 1245 (Figure 3(e)) and the expansion continued through 1345 (Figure 3(g)) and 1445 (Figure 3(i)), by which time another line of deep convection had broken out on its southern flank which developed into the separate MCS labelled D.

The corresponding sequence of hourly radar-network pictures from 1045 to 1445 is shown in Figures 3(b), (d), (f), (h), (j) with outlines of the parallax-corrected visible anvil of MCS C superimposed. Although the extent of precipitation increased throughout the period, its maximum intensity

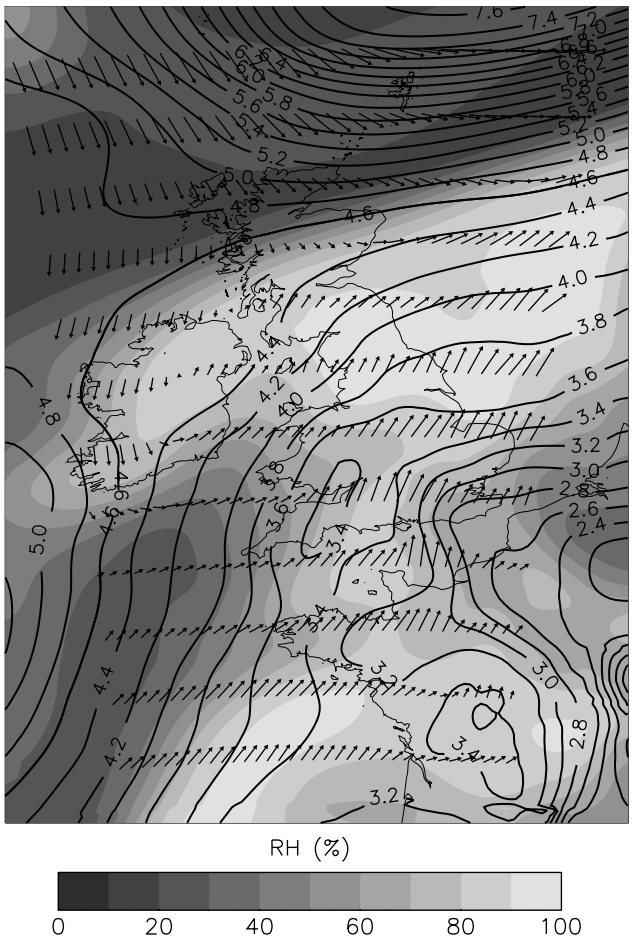

Figure 2. Isentropic analysis at 1200 UTC, 24 June 2005, derived from Unified Model output. This shows air flow on the 32 °C theta surface (contours at 0.2 km height intervals) and relative humidities on this surface (grey shading). (Comparison with the radiosonde ascent in Figure 4 indicates that the Unified Model overestimates the height of this surface by 1 km at Swanage in southern England.)

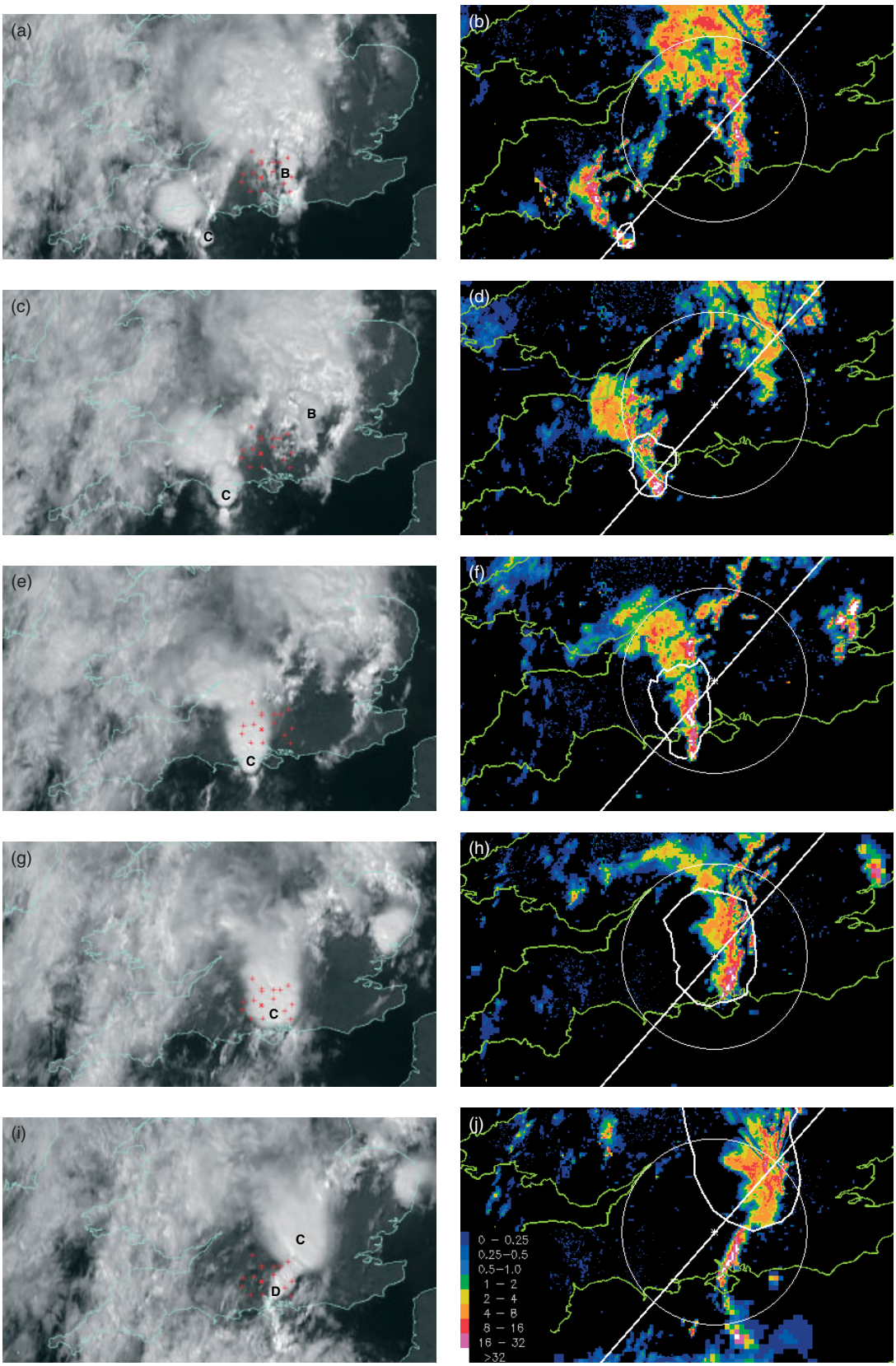

Figure 3. (a, c, e, g, i) MSG high-resolution visible images and (b, d, f, h, j) radar-rainfall plots from the weather radar network over parts of southern England and Wales at (a, b) 1045, (c, d) 1145, (e, f) 1245, (g, h) 1345 and (i, j) 1445 UTC, 24 June 2005. MCSs B, C and D are labelled on the satellite images, which are not adjusted for parallax. Also shown on the satellite images are the locations of the automatic weather stations set up for CSIP (red +). The radar-network images are composites with resolutions of 1,2 and 5 km, depending on radar range; colours represent retrieved rainfall intensities as given by the key. The parallax-corrected outline of the visible anvil from MCS C has been superimposed on the radar plots. The circles show the 95 km range of the Chilbolton Doppler radar (not one of the network radars). The line, through Chilbolton and orientated southwest to northeast, shows the track of MCS C as it first approached and then receded from Chilbolton.

remained above a peak radar threshold of 32 mm h^{-1} until 1345, after which it rapidly weakened.

The white outline depicting the anvil canopy of MCS C in the sequence of radar pictures in Figure 3 shows that the MCS as a whole travelled in a southwest to northeast direction, along the white line and taking it directly over the Chilbolton radar. However, the overall anvil canopy was generated and sustained by a roughly north – south orientated line of convection in which new cells continually formed at the southern end and decayed towards the northern end. Radar scans along the direction of the white line, which are presented later in section 3, reveal a decreasing trend in convective vigour with time. This is partly due to the weakening of the overall MCS with time, but is also influenced by the tendency for the more active convection to occur to the south of the white line at the later times.

2.2. *Thermodynamic structure in the near environment of MCS C*

Figure 4 shows data from a radiosonde launched at 1100 within the inflow towards the MCS C updraught. This is the system analyzed in detail in section 3. The lowest kilometre of the atmosphere is seen to have been characterized by air too cool to be able to feed any deep updraughts (Figures 4(a) and (b)); this cool air was associated with a northeasterly low-level jet on the northern side of the low, with a speed of typically 12 m s^{-1} (Figure 4(c)). We shall refer to this as an undercurrent. Parker (2008), in his modelling study of an MCS with elevated convection, identified a similar undercurrent which he referred to as an 'underflow regime'.

The cool undercurrent was capped by an approximately isothermal layer between 1.0 and 1.6 km (900 to 830 hPa). Above this was a warm, almost dry-adiabatic, layer up to around 2.0 km (800 hPa) with a theta of 31 °C. Above this, centred at 2.3 km (770 hPa), was a moist layer of high wet-bulb potential temperature (theta-w) (this is later identified as Flow 4 in section 3.1). The analysis of flow on the 32 °C theta-surface, presented earlier in Figure 2, shows that the MCS was within a belt of moist air (a warm conveyor belt on the eastern edge of a cold-frontal zone) that extended northnortheastwards from the western side of the Iberian peninsular. Figure 4(a) shows that the moist air in the warm conveyor belt at 2.3 km (770 hPa) was characterized by a theta-w as high as 18 °C; such air had the potential to ascend buoyantly to around 250 hPa with typical temperature excesses of around 2 °C (convective available potential energy, CAPE=405 J kg^{-1}), provided it could overcome a layer of convective inhibition (CIN) centred at 740 hPa (CIN=70 J kg^{-1}).

Another moist layer with high theta-w (18 °C) can be seen in Figure 4(a) embedded within the stable layer at 1.3 km (870 hPa). (This is identified as Flow 2 in section 3.1). This required much greater lifting to overcome a considerable amount of CIN (263 J kg^{-1}) before it could undergo deep convection (CAPE=399 J kg^{-1}). The later analysis in section 3.1 suggests that local processes within the storm may have been able to provide the necessary lifting once the storm had developed. (It is not within the scope of this paper to examine in detail the lifting mechanisms responsible for the actual initiation of the MCS.) To clarify the precise depths of the layers that were capable of achieving buoyancy, the data in Figure 4(a) have been re-plotted in Figure 4(b) to show theta-w and also theta-s as a function of height. (The environmental theta-s at any given level is the dry-bulb temperature read off along a saturated pseudo-adiabatic curve (Ludlam, 1980, Chapter 3); neglecting water loading, a parcel is buoyant if its theta-w when lifted exceeds the theta-s of the environmental air at the new level.) Figure 4(b) will be referred to again in section 3.1.

The southwesterly winds increased with height over the depth of the convection, reaching 20 m s^{-1} in the upper troposphere (Figure 4(c)). The MCSs that developed within the CSIP area travelled from the southwest at typically 15 m s^{-1}. The air of high theta-w that fed the elevated convection had a southwesterly component of velocity that was somewhat less than 15 m s^{-1} and so this air was ingested at the leading edge, albeit with a component from the right (southeast). At the storm tops, the air from the convective updraughts spread outwards in all directions but predominantly ahead of the storm. Relative to the advancing storm, the cool stable air flow beneath the storm travelled very rapidly against the storm's direction of travel. Except on a few rare occasions, there was no evidence from the Doppler radar of sharp horizontal gradients of wind extending down to the ground from any of the main storms. This indicates that downdraughts from above the stable layer were, for the most part, not penetrating to the surface through the cool low-level undercurrent. Nevertheless, as shown next, the passage of MCS C and the other MCSs, whilst not producing strong surface winds, did lead to significant perturbations that were detected at the surface.

2.3. *Surface weather associated with the passage of the MCSs*

Twelve automatic weather stations were operational within a 50 km radius of Chilbolton and their locations are shown in Figure 3 (and Figure 6). All the AWSs showed a remarkably similar sequence of events as a number of MCSs passed overhead at roughly 3 h intervals. The traces of pressure, temperature, relative humidity, and wind speed and direction at one of these stations are shown in Figure 5. Three MCSs are labelled: A, B and C. Each of these MCSs produced a positive pressure anomaly of typically 2 hPa, accompanied by oscillations of 2 to 5 °C in temperature and 20 to 30% in relative humidity. Many of the stations experienced a shift in the winds from east of north to west of north during the passage of some of the pressure anomalies and some also experienced lulls in the wind speed. Rarely were there strong gusts as would have been expected if there had been pronounced density currents. According to Maddox (1980), who studied large MCSs which he called mesoscale convective complexes, this is a characteristic feature of such MCSs. The low-level winds, and also the anomalies in surface temperature and humidity, will be investigated in detail in another paper as part of a more detailed analysis of the wave in the undercurrent that occurred in the present MCS. Suffice it to say here that evaporation within the undercurrent and the effects of cloud shadowing (e.g. Marsham *et al.*, 2007a, b) probably played a role in addition to any possible effects of the descending air within the slantwise circulations. The nature of the slantwise circulations and their association with the undercurrent wave will be the main focus of the present paper.

An analysis of the time of arrival of the pressure maximum associated with MCS C (Figure 6) is consistent

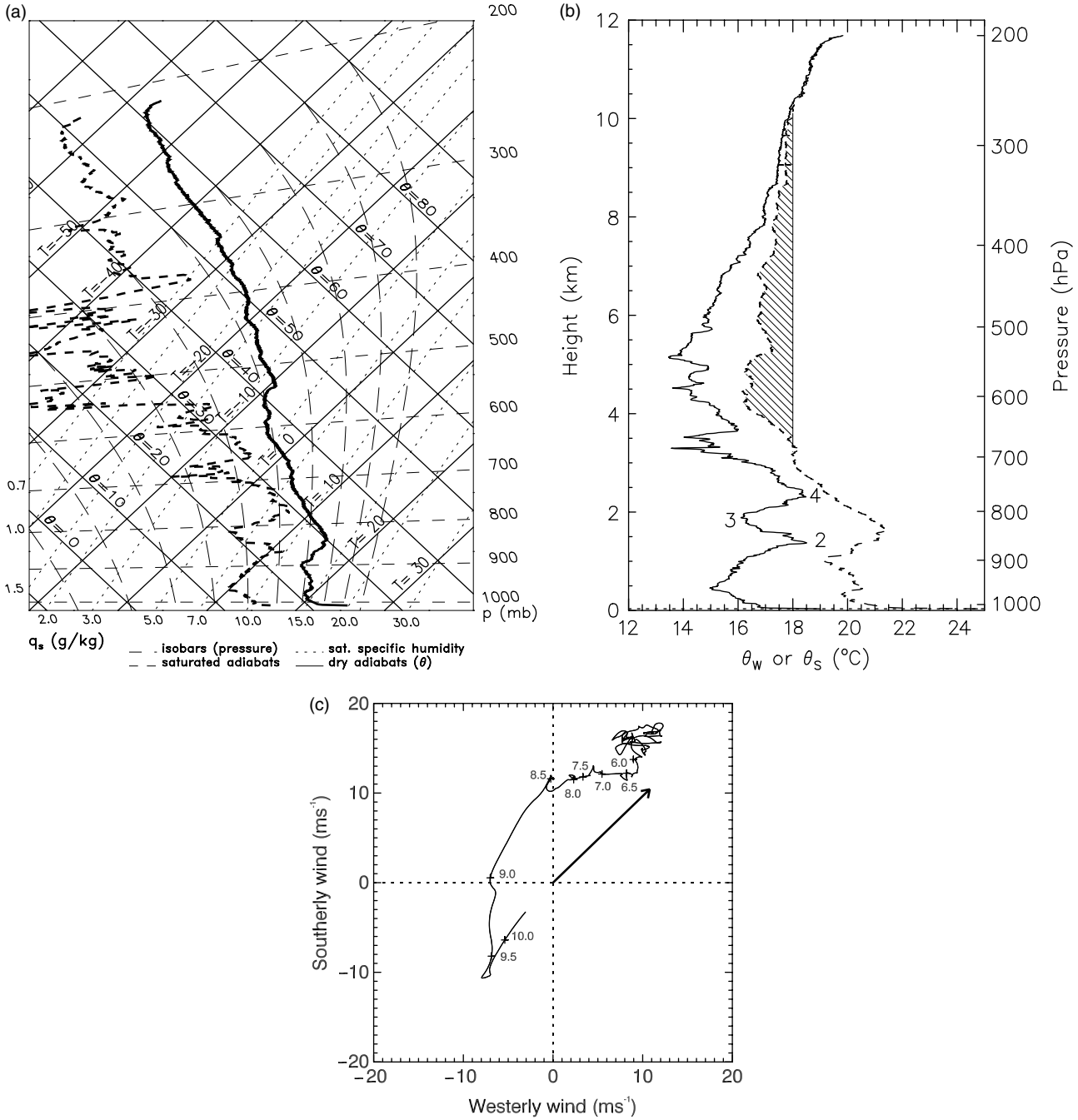

Figure 4. Data from the Swanage radiosonde launched at 1100 UTC, 24 June 2005: (a) tephigram, (b) theta-w (solid curve) and theta-s (dashed curve) plotted as a function of height, (c) wind hodograph, with pressure values labelled in hundreds of hPa. Hatching in (b) denotes heights of positive buoyancy for parcels ascending adiabatically from either of the two layers of high theta-w; these layers are labelled 2 and 4 to correspond to the flow identification scheme adopted in section 3.1, and the dry layer in between is labelled 3 for the same reason. The arrow in (c) denotes the 15 m s^{-1} velocity of MCS C towards the northeast. The location of the Swanage radiosonde site is plotted in Figure 6.

with the storm and associated surface effects travelling from the southwest at 15 m s^{-1}. The typically 45 min duration of MCS C's overall pressure anomaly at each station corresponds to the passage of an anomaly 40 km or so across. The magnitude of the pressure anomaly tended to increase with time, being about 1.5 hPa at 1235 and 3 hPa by 1405; although the magnitude would obviously have been influenced by the evaporative cooling, it would also have been affected by the structure of the wave, which, as we shall show, led to local variations in the depth of the cool undercurrent and overlying stable layer.

2.4. *Overview of the rear-inflow jet associated with MCS C*

The location and coverage of the Chilbolton radar was shown in Figure 3. This radar was making sequences of low-elevation PPI (plan – position indicator) scans and RHI (range – height indicator) scans at nominally 20° intervals of azimuth, repeated typically every 38 min. It can be seen from Figure 3 that MCS C followed a track that took it almost directly over the radar. This is important for the analysis because it means that Doppler scans through the centre of the storm as it approached and receded from the radar provide information on the component of the wind

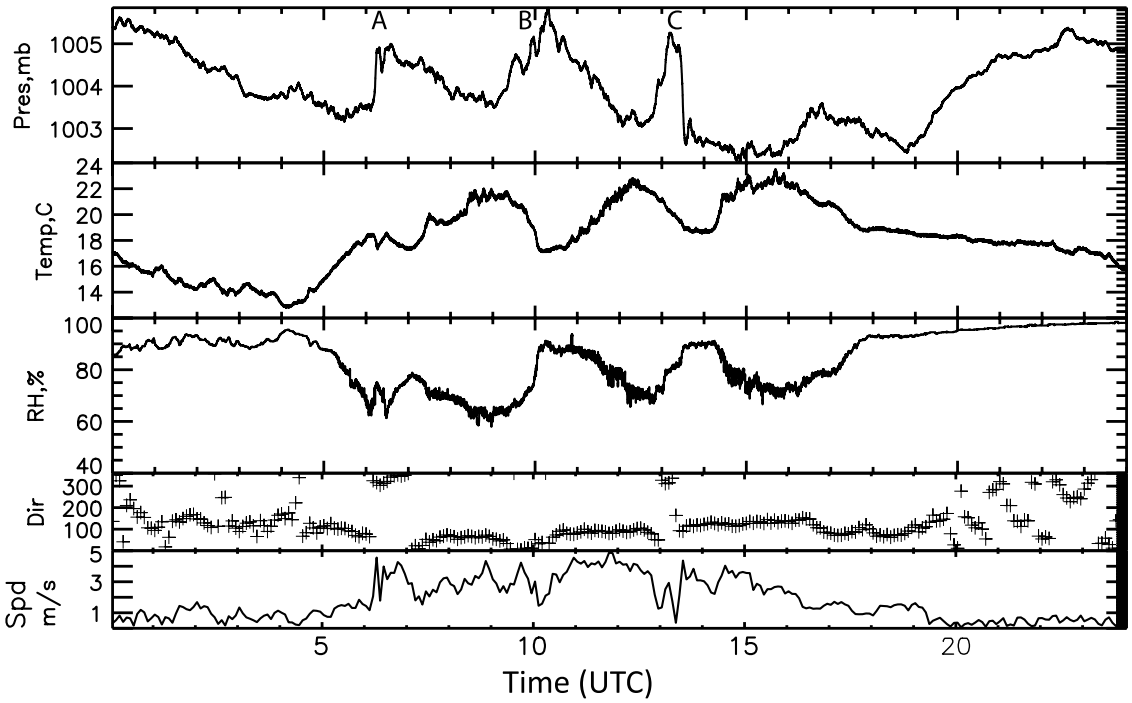

Figure 5. Traces of pressure, temperature, relative humidity, and wind direction and speed for the automatic weather station at Chilbolton (site 26) on 24 June 2005; mesoscale surface pressure maxima associated with MCSs A, B and C occurred at 0630, 1020 and 1315 UTC, respectively. The location of the Chilbolton site is shown by the asterisk in Figure 6.

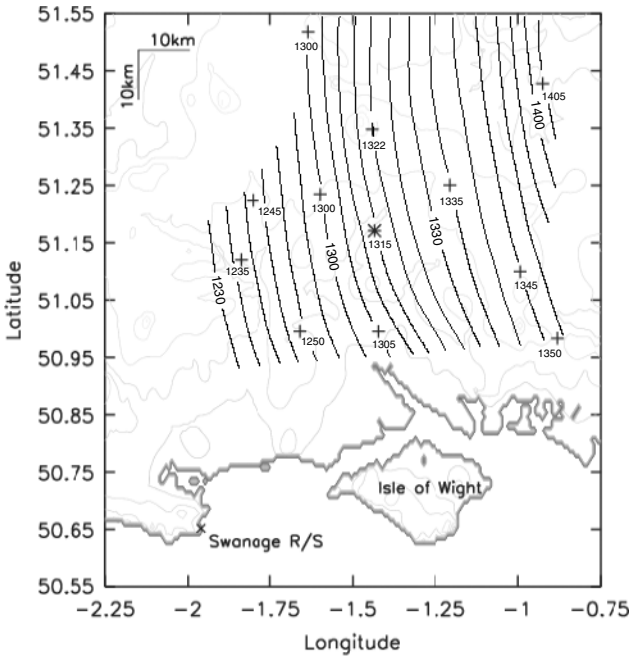

Figure 6. Time of passage of the pressure maximum from MCS C derived from 12 AWSs in the CSIP area, the locations of which are plotted in Figure 3. The asterisk denotes the position of Chilbolton. The orography is shown by the grey contours with 50 m spacings.

parallel to the storm's direction of travel: i.e. the analysis is essentially two-dimensional. Key features that these scans can identify are the slantwise circulations, consisting of layers of sloping storm-relative rearward-flowing ascent and forward-flowing descent. We shall be showing in section 3 that these layers of ascent and descent are manifested in the Doppler radar scans as coherent sloping layers of storm-relative Doppler velocities separated by coherent sloping layers of high shear and spectral width. If such layers had been present in Doppler radar scans at only one time, we would not have been justified in identifying them unambiguously with corresponding ascending and descending limbs within a system of organized slantwise circulations. However, we show radar scans at four times over a 2.5 h period, and the coherent sloping layers of storm-relative flow are seen to be present at each time, albeit with somewhat different slopes. Because of the persistence of the overall flow configuration, we are therefore confident in the reality of the inferred layers of ascent and descent. One of these flows, the lowermost layer of slantwise descent, corresponded to a rear-inflow jet as discussed in the Introduction.

The axis of the rear-inflow jet, inferred from the sloping zone of strong rear-to-front air flow in the RHI scans, was identified along a number of azimuths close to the storm during scans centred on the four times (1153, 1233, 1312 and 1423) as the storm approached from the southwest and later receded towards the northeast of the Chilbolton radar. The height of the layer corresponding to the rear-inflow jet could be clearly identified from the RHI scans along three or four azimuths at each of these times, from which it has been possible to map both the orientation and the slope of this layer, as shown in Figure 7 for all four times. At 1153 the layer can be seen sloping down from 5 to 3 km over a 30 km wide front, with a slope of about 1 in 3.5. A slope of 1 in 4.5 is evident at 1233, by which time it can be seen extending down to 2 km. The rear-inflow jet did not extend much lower than this because the cool undercurrent apparently acted as a barrier. The slantwise ascent overlying the rear-inflow jet underwent a similar evolution in slope to that of the rear-inflow jet. By 1312 the slope of the rear-inflow jet is seen to have decreased to about 1 in 6($\pm$1). An even gentler slope, of 1 in 9($\pm$1) was evident by 1423. The pressure maximum measured at the

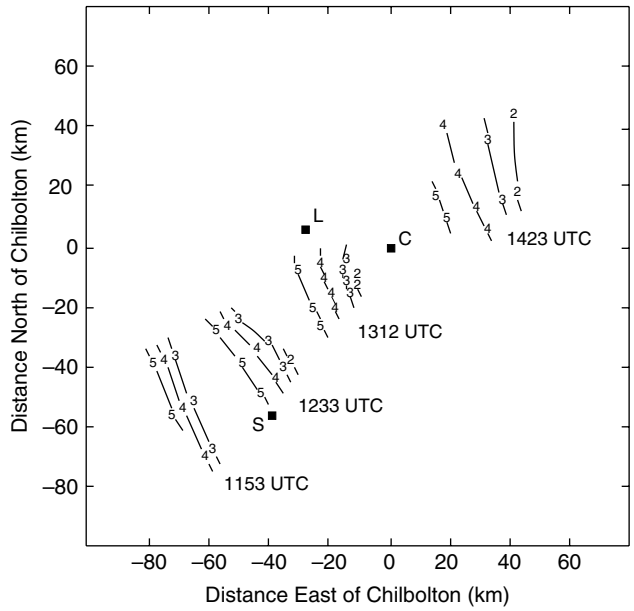

Figure 7. Contours of the height of the midpoint of the layer of slantwise descent within MCS C corresponding to the rear-inflow jet, as derived from the Doppler radar at Chilbolton. Isopleths are drawn at 1 km intervals from 5 km down to 2 or 3 km at four times: 1153, 1233, 1312 and 1423 UTC, 24 June 2005. The digits 2, 3, 4 and 5 represent the actual data points along the azimuths observed during those RHI scans that intersected the core of the storm, (small positional adjustments have been made to allow for non-simultaneity of successive scans). Also shown are the locations of Chilbolton (C), Swanage (S) and Larkhill (L) where radiosondes were released.

ground was close to the nose of the overrunning rear-inflow jet throughout.

The next section analyses two-dimensionally the detailed structure of MCS C as the slantwise circulations evolved. It presents a unique set of observations showing the way in which the rear-inflow jet is associated with a wave in the undercurrent.

It is worth stressing that a key assumption throughout this paper is that coherent sloping layers of positive and negative system-relative flows do indeed correspond to coherent slantwise downdraughts and updraughts, respectively, i.e. the boundaries of these flows are not merely regions where horizontal flows either accelerate or decelerate as they cross them. As noted above, this interpretation is supported by the fact that these boundaries are defined by coherent layers of high spectral width as well as by coherent layers of strong shear separating the main flows. Moreover, the locations of sloping updraughts and downdraughts inferred in this manner are found to be consistent with high and low values, respectively, of theta-w inferred from the radar bright band and nearby radiosondes. Over the period from 1153 to 1423, Figure 7 shows that the axis of the descending rear-inflow jet travelled at between 15 and 16 m s^{-1} at heights from 2 to 3 km and between 13 and 14 m s^{-1} at heights from 4 to 5 km. Given that the resolved component of flow along much of the rear-inflow jet exceeded 20 m s^{-1} relative to the ground, i.e. typically over 5 m s^{-1} faster than the interface with the overlying sloping updraught with its typical slope of 1 in 5, then the air in much of the rear-inflow jet can be inferred to have been descending strongly, at about 1 m s^{-1}.

3. Structure of the evolving MCS as observed by the Chilbolton radar

3.1. RHI scan at 1155 UTC: a time of vigorous convection with steeply inclined slantwise circulations.

The analysis in this subsection is based on the radar RHI data at 1155 (Figure 8) together with data from two nearby radiosondes, one just ahead of and the other just behind the storm. The inferences drawn from them are synthesized in Figure 9. The reader may find it helpful to refer ahead briefly to Figure 9 to see where the following analysis of Figure 8 is leading.

Figures 8(a), (b) and (c) show three different parameters from the Chilbolton radar for the scan at 1155 along 221°, looking towards the core of MCS C as it approached the radar at long range. This corresponded to the time when the precipitation intensity from the MCS had reached its maximum value, and the reflectivity plot in Figure 8(a) shows the intense precipitation centred near 80 km. Anvil echo extends ahead of the storm to about 40 km from the radar but the rear edge of the anvil is just beyond radar range. Ahead of the storm, multiple layers of low-reflectivity echo can be seen at low levels. These echo layers are due to backscatter from insects and/or Bragg scatter from refractivity inhomogeneities; either way, they are an indication of statically stable layering since insects are known to congregate at local temperature maxima such as at the top of inversions (e.g. Reynolds *et al.*, 2008). There are traces of echo from the stable layers out to 59 km from the radar but beyond this the clear-air echo is outside detectable range.

Radiosondes were released hourly from Swanage, which is situated close to the RHI section at a range of 71 km. Data from one of these sondes, released at 1100, was shown earlier in Figure 4. The storm-relative position of this sonde places it ahead of the storm at a radar range of 22 km at 1155 where, according to the reflectivity scan in Figure 8(a), the stable layering was between 1.0 and 2.0 km, the three strongest layers being between 1.0 and 1.7 km. Figure 4(a) is consistent with this, showing a broadly isothermal layer between 1.0 and 1.7 km (900 to 830 hPa); there is even evidence of sub-structure within the isothermal layer corresponding to the three individual strong echo layers in Figure 8(a). Below these, at heights ranging from 100 to 300 m, there is another, rather less stratiform, echo layer corresponding to the top of the shallow convective boundary layer, as shown in Figure 4(a). The close correspondence between the clear-air layer echoes and the stable layers measured by the radiosonde argues in favour of the layer echoes being due to Bragg scattering. However, the Chilbolton radar obtained measurements of differential reflectivity (not shown) which gave values of up to 5 dB in the stratified layers compared to less than 1 dB in the convective 'clear-air' echoes. Such high values of differential reflectivity could be due to elongated insects or, if due to Bragg scattering, would indicate unusually anisotropic scatterers, perhaps because the refractive-index inhomogeneities were being generated within very highly sheared layers. The layering extends between heights of about 1.3 and 2.0 km at 10 km range but lowers steadily along the direction of flow towards the storm, being between 1.0 and 1.5 km at 45 km. This is indicative of a general region of descent immediately ahead of the storm, as was also inferred behind the storm from the cloud-free zone remarked on in connection with the satellite

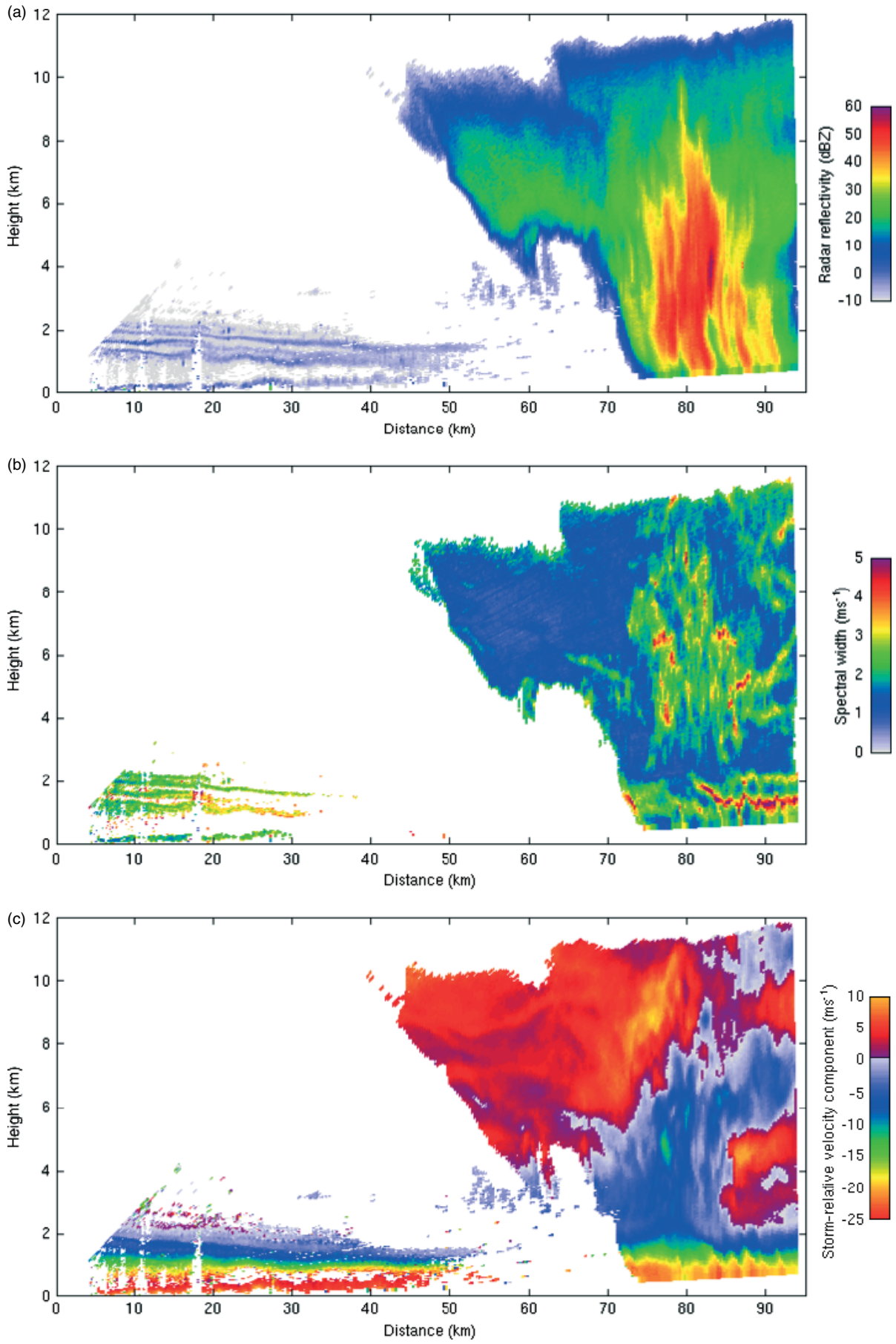

Figure 8. RHI scan from the Chilbolton radar along 221° at 1155 UTC, 24 June 2005: (a) reflectivity (dBz), (b) spectral width (m s^{-1}), and (c) Doppler (line-of-sight) velocity (m s^{-1}), with the colour key labelled in terms of storm-relative velocities; red and orange colours are duplicated, corresponding to negative velocities below 2 km and positive velocities above 2 km. Positive velocities are in the direction the storm is travelling (from right to left). The undercurrent gravity wave was situated between radar ranges 60 and 90 km.

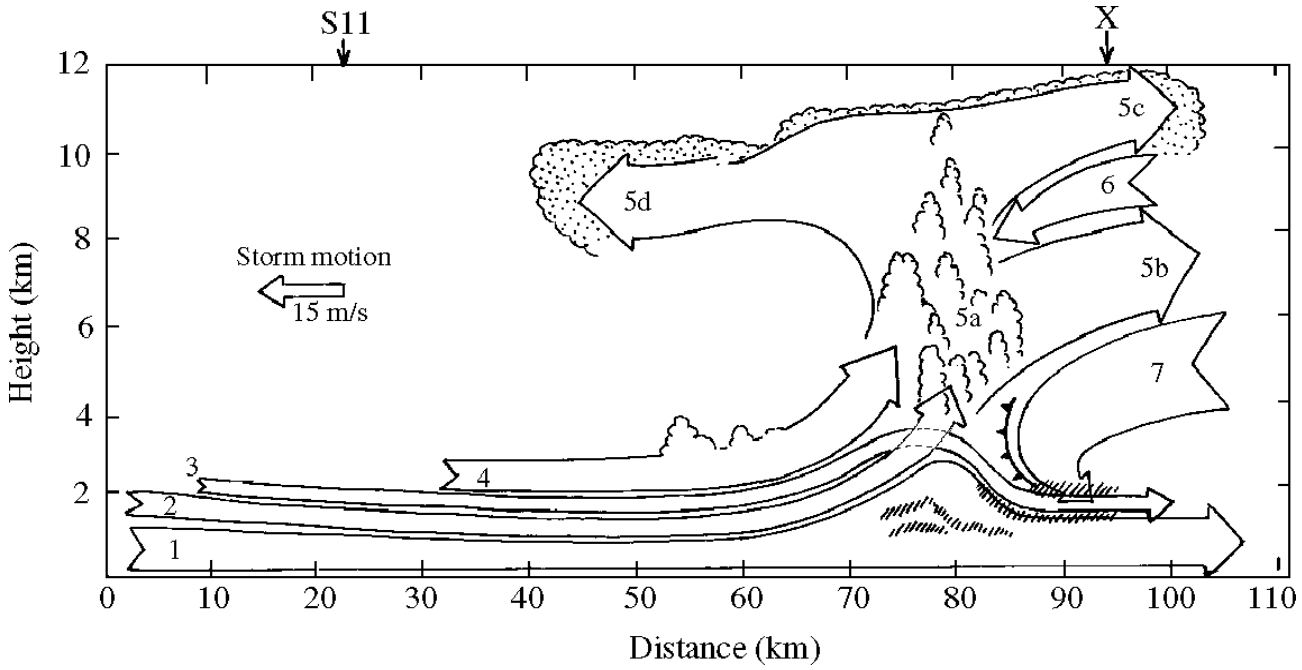

Figure 9. Synthesis of inferences drawn from Figures 8(a), (b) and (c) and from radiosondes launched at 1100 and 1300 UTC from Swanage, which was situated within the section at 71 km range. The label S11 indicates the storm-relative position of the 1100 sonde. The storm-relative position of the 1300 sonde is to the right of the diagram at 130 km range. The coverage of the diagram corresponds to that of Figures 8 out to the range marked X but is extended to 110 km to enable the overall extent of the satellite-determined anvil cloud to be indicated (crenellated lines with dotted shading). Open arrows represent flow relative to the MCS which was travelling at 15 m s^{-1} from right to left. The text gives an explanation of these flows. The arrow labelled 7, approaching from the right, is the rear-inflow jet, the leading edge of which is indicated by cold-frontal symbols. The arrow representing Flow 3 is drawn dotted where it may perhaps have been penetrated by convective parcels fed by Flow 2. The amount of deepening of Flow 1 within the wave is uncertain and may be exaggerated in this diagram. The convective plumes drawn in the middle and upper troposphere, and the hatched layers of strong shear and/or turbulent mixing at low levels beyond 70 km, have been inferred from the spectral width in Figure 8(b). Layers of high spectral width also separate Flows 5c, 6, 5b and 7. (These features are depicted more clearly at the later time of 1233 – see section 3.2 – when the entire storm had come within radar range.)

image in Figure 3(c). This inference is secure if the layers were indeed due to Bragg scattering, but would be somewhat less so if the layers were due to insects congregating within the stable layers, because one could not rule out the possibility of the insects systematically departing from the original stable layers as they approached the storm.

Although it is impossible to gain any insight into the stable stratification of the atmosphere directly under the storm from the reflectivity plot in Figure 8(a), it is possible instead to use the plot in Figure 8(b) for this purpose where it shows layers of high spectral width within the precipitation echo. These layers are associated with regions of strong shear, and probably shear-induced turbulence too, the strong shear being sustainable because of strong static stability. These layers – especially the green, yellow and red layer with a spectral width of up to about 4 m s^{-1} which lowers from 2.3 km at 80 km to 1.4 km beyond 85 km – are highly distorted compared with the gently sloping layers ahead of the storm. The reason for this will be clarified shortly.

The most intense echo in Figure 8(a) ($Z \simeq 55$ dBz) was associated with heavy precipitation generated by vigorous (upright) convection. The boundaries of individual convective plumes show up in Figure 8(b) as mantle-shaped patterns[†] of high spectral width owing to high turbulence intensity and/or velocity gradients at the edge of the plumes. It is one of the benefits of the Chilbolton radar that the narrowness of its beamwidth enables such boundaries to be resolved easily even at long ranges. By superimposing a tracing of Figure 8(b) on top of Figure 8(a), it can be seen that the tops of individual convective plumes identified from the mantle-shaped maxima in spectral width tend to be associated with the tops of individual streamers of maximum reflectivity due to hydrometeors newly grown within each convective plume. It is significant that the boundaries of convective plumes identified in Figure 8(b) can be seen extending up to and above 10 km but generally do not extend much below 3 km. This is because, as shown by Figure 4(b), air with a sufficiently high theta-w ($> 17\,^{\circ}$C) to achieve buoyancy upon lifting was located within two layers, from 2.1 to 2.9 km (790 to 710 hPa) and 1.2 to 1.6 km (880 to 840 hPa), neither of which could become significantly buoyant until it had been lifted above 700 hPa (3 km). Figure 4(b) shows that, in the case of the upper layer of high theta-w, lifting of 0.4 km was required to overcome the CIN, whilst for the lower layer as much as 1.4 km of lift was required since the CIN in this case was substantial.

The wind hodograph in Figure 4(c) shows that, just ahead of the storm at 22 km radar range, both layers of air with high theta-w (ie the layers 790 – 710 hPa and 880 – 840 hPa) had a component of velocity from the northeast relative to the storm, which at this time was travelling at 15 m s^{-1} from the southwest. Thus the convective updraughts would have been derived from air approaching the front of the storm (ie from the left-hand side of Figure 8) at a relative velocity of between 2 and 16 m s^{-1}. This is consistent with the Doppler RHI scan

[†]These patterns are somewhat analogous to the mantle-shaped reflectivity patterns that in other circumstances can be seen in the absence of precipitation echo, in that case because of the effect of turbulence on the refractivity gradients at the boundaries of the convective plumes.

in Figure 8(c)[‡] which shows that this inflowing air (mostly shaded blue, with some green) continued to flow rearwards relative to the storm as it ascended in a slantwise manner between radar ranges of 70 and 95 km, albeit with some of the air parcels ascending more rapidly towards the storm top within the convective plumes shown by the mantle echoes in Figure 8(b). Although the upper layer of high-theta-w inflow would have convected more readily because it was subjected to the smaller CIN, there is some tentative evidence that the lower layer may have contributed to the convection as well. In particular, the small patch of green in Figure 8(c), centred at 78 km range and 4.8 km height, corresponding to air with a storm-relative velocity characteristic of the lower inflow layer, was associated with one of the mantle shaped convective plumes in Fig 8(b), suggesting that at least some of the convection may have been due to the lower-level inflow, notwithstanding the high CIN.

The tallest convective plumes were at 80 km range and, where they penetrated above 10 km altitude, they produced a divergent anvil outflow, with some air travelling rearwards relative to the storm (blue in Figure 8(c)) and some travelling ahead of the storm along with the upper-level environmental flow (red shading). The small orange areas in Figure 8(c) between 7.5 and 11 km height and 73 and 78 km range correspond to even stronger flow away from the storm (right to left), with storm-relative velocities of about 10 m s^{-1}. These areas are situated at the leading edges of the individual convective turrets outlined by the regions of high spectral width in Figure 8(b). The associated narrow regions of horizontal divergence on the right-hand edges of these orange areas in Figure 8(c) are indicative of where the updraught plumes are decelerating and beginning to feed the forward outflow.

Figures 4(a) and (b) show that there was a stable layer between 6.8 and 7.5 km (ie just below 400 hPa). Although air from the entire depth of the layers 1.2 – 1.6 km and 2.1 – 2.9 km had a high enough theta-w to acquire some buoyancy when lifted sufficiently, only the air in these layers with a theta-w exceeding 17.5 °C would have been able to ascend buoyantly above 7.5 km, and then only in the undiluted cores of the convective plumes. Indeed, it appears from Figure 8(c) that much of this air, ascending as a slanting updraught, did leave the storm (as a rearward flow) at a height of around 7(±1) km.

Beneath this slantwise updraught, and also beneath the overlying anvil outflow at the rear of the storm, there is evidence of two layers of inflow from the rear (red shading), one between 8 and 10 km height and the other between 3 and 6 km. We believe that the air in these layers of inflow from the rear was descending slantwise, an interpretation which may not be obvious at this time but, as discussed in section 3.2, was more convincing later when the storm came fully within radar range and a larger extent of these inclined flows could be seen. The lowermost red layer, between 3 and 6 km height in Figure 8(c), corresponds to the main rear-inflow jet which is seen to have terminated not at the surface but, rather, just above 2 km at a radar range of 85 km. A radiosonde released from Swanage at 1300 (not shown) was situated 45 km behind the leading edge (nose) of this rear-inflow jet at an effective radar range of 130 km. The sounding showed a layer of air between 4 and 6 km (620 to 480 hPa) with rather low theta-w, between 15 and 16 °C, approaching the rear of the storm with a small relative velocity (up to 3 m s^{-1}); this is probably the air that fed the rear-inflow jet. According to the Doppler information in Figure 8(c) the rear-to-front component of this flow, relative to the storm, increased within the storm, to about 10 m s^{-1} just behind its nose (at 87 km range).

In the cool low-level flow beneath 2 km (800 hPa), both the Doppler data in Figure 8(c) and the nearby radiosondes (e.g. Figure 4(c)), as mentioned earlier, show air travelling very strongly rearwards relative to the advancing storm. The storm-relative rearward component is seen to have been as much as 25 m s^{-1} in places within the undercurrent below about 1 km. Ahead of the storm, Figure 8(c) shows that the velocity contours are smoothly layered, albeit descending gently towards the storm roughly in line with the descending flow previously inferred from the sloping reflectivity layers in Figure 8(a). Beneath the storm itself, however, the velocity contours, especially the green-blue boundary, are distorted in a manner broadly consistent with, but rather less than, the distorted layers of high spectral width seen in Figure 8(b). The fact that the vertical perturbations in the velocity contours are less than that of the spectral-width layers is due to a deceleration in the flow where it deepens. That is to say, the velocity contours underestimate the true vertical perturbation of the streamlines in the undercurrent flow.

Two factors are particularly noteworthy. The first is that, at the leading edge of the storm, close to 75 km radar range, Figure 8(c) shows the depth of the cool high-speed rearward undercurrent flow (red and yellow) to have been at least 50% greater than it was farther ahead of the storm, at 30 km, say. Since, for the reason given above, the vertical displacement of the velocity contours underestimates the true vertical perturbation in the flow, the deepening of the undercurrent was even greater than this. This increase in depth may be a manifestation of the wave-like behaviour. Secondly, the velocity of the high-speed flow became more variable at ranges beyond 78 km, suggesting 'eddies' with a wavelength of 2 km. The pattern of the radar wind-shear plot (not shown) suggests that these eddies may have been Kelvin – Helmholtz billows with crest-to-trough amplitude up to 400 m. We hypothesize that the triggering of the billows was due to a local increase in the already strong shear, caused by the impact of the rear-inflow jet at the top of the stable layer increasing the depth and decreasing the velocity of the cool low-level undercurrent just ahead of it whilst decreasing the depth and increasing the velocity of the undercurrent directly beneath it. The local increase in shear in the vicinity of the billows is examined in section 3.2 in the light of better data at a later time and so we do not pursue it further here.

The above inferences, made from RHI data and the Swanage radiosondes at 1100 and 1300, are synthesized in the vertical section shown in Figure 9. The storm-relative position of the 1100 sounding is indicated in Figure 9 by the label S11; the storm-relative position of the 1300 sounding was at 130 km range (not shown). Seven flows are identified in Figure 9. The flows have been drawn as a fairly precise overlay, consistent with the detailed attributes of Figures 8(a), (b) and (c) discussed above. However, the

[‡]Note that the colours in the Doppler RHIs in Figures 8(c) and 11(a) refer to radial velocities relative to the storm, with positive velocities in the direction of storm travel, i.e. towards the radar. The colours, orange and red, are used twice, corresponding to velocities in the direction of storm travel above 2 km and against the direction of storm travel below 2 km.

form of the flow shown in Figure 9 is conjectural in some places where indicated below. This is particularly so in the case of the flow near the undercurrent wave, in the lowest 3 km, where the configuration should be regarded as highly schematic.

Flow 1: An undercurrent of cool air (theta-w between 15 and 17 °C according to Figure 4(b)) flowing against the storm's direction of travel with a storm-relative velocity of up to 25 m s^{-1} (Figure 4(c)). The layering in reflectivity ahead of the storm (Figure 8(a)) shows the top of the undercurrent initially descending as it approached the storm at radar ranges between about 5 and 50 km, albeit with some deepening of the shallow convective boundary layer within it. Beyond 73 km, within the storm, the shape of the layering in spectral width (Figure 8(b)) is indicative of some overall deepening of the undercurrent out to 78 km, as part of a wave. Beyond 78 km the depth of the undercurrent is seen to decrease again. Because the Flow-1 arrow is based on reflectivity data at close range and spectral width at long range, with no overlap in these two data sources (indeed there is a gap between them), the way in which the two ends of this flow arrow have been connected in Figure 9, and in particular the degree of deepening of the flow in the region of the wave, is conjectural. It is clear that there is some deepening of the undercurrent in this region but it is possible that the magnitude of the deepening was less than that portrayed in Figure 9.

Flow 2: Part of a very stably stratified flow with theta-w between 17 and 18 °C having a strong storm-relative inflow velocity. This is the lower of the two layers of high theta-w, centred at 1.4 km, as shown in Figure 4(b). The layering in reflectivity shows that, like the undercurrent, this flow first descended as it approached the storm. It then ascended above the elevated head of undercurrent air and, despite the high CIN, it may have fed some of the upright convection, depicted in Figure 9 by the cloud turrets (labelled 5a) traced from the spectral-width plot. However, forced ascent through more than 1.4 km would have been required for Flow 2 to have overcome the convective inhibition imposed by Flows 3 and 4 (although Flow 4 was itself undergoing convection – see below).

Flow 3: A shallow layer of warm but dry air with relatively low theta-w (16.3 – 17 °C) which capped Flow 2. Like Flows 1 and 2, it would have ascended close to the storm, whereupon it may have been penetrated by the buoyant air parcels from Flow 2 before descending at the top of the undercurrent (Flow 1) and probably mixing with it and Flow 7 coming from above (in the hatched regions of large spectral width in Figure 9).

Flow 4: A further layer of air with high theta-w (17 – 18 °C), which was situated between 2.1 and 2.9 km at the position of the 1100 radiosonde, i.e. the upper layer of high theta-w in Figure 4(b). This had a smaller storm-relative inflow velocity than the underlying flow; indeed, whilst the radiosonde showed an inflow velocity of about 3 m s^{-1} at 1100, the Doppler data (Figure 8(c)) show that the relative velocity had decreased to zero at this location by the time of the RHI scan, developing some component of inflow only closer to the storm, as represented in Figure 9 by the delayed start of the Flow 4 arrow. The high theta-w air of Flow 4 would probably have been the main contributor to the upright convection, as shown, because it required lifting of only 0.4 km to overcome the CIN.

Flow 5: Air fed by Flows 2 and 4 which ascended as upright convection (5a) and then peeled off at mid-levels as rearward-sloping ascent (5b) and in the upper troposphere as a divergent outflow behind (5c) and ahead of (5d) the storm. Only the relatively undiluted cores of the convective updraughts are likely to have fed the upper-tropospheric outflows.

Flow 6: A weakly descending slantwise flow beneath the rear part of the upper-level anvil outflow.

Flow 7: A slantwise-descending flow of cold air, with theta-w mainly between 15 and 16 °C at altitudes between 4 and 6 km, entering the storm beneath Flow 5b and corresponding to a rear-inflow jet (red in Figure 8(c)), with a relative inflow velocity of up to 10 m s^{-1} near its leading edge. The shape of Flow 7 above the impact zone, where it is drawn curving around, is conjectural; parts of this region (hatched region of large spectral width in Figure 9) would probably have experienced strong mixing.

3.2. RHI scan at 1233 UTC: weaker convection but still well-defined steep slantwise circulations.

Thirty-eight minutes later, when MCS C was next scanned by the Chilbolton radar, the available RHI scans were on the northern edge of the storm core and so the observed upright convection was weaker. This is shown by the absence of tall columns of high reflectivity in the RHI scan (Figure 10(a) compared with Figure 8(a)) and by the reduced extent of mantle-shaped regions of high spectral width within the mid-troposphere (Figure 10(b) compared with Figure 8(b)). In contrast, as we shall show shortly, the slantwise circulations seen in this scan were undiminished.

We saw in Figure 8(a) that, 60 km ahead of the storm, the stable layering occupied the height interval from 1.3 to 2.0 km but descended to 1.0 – 1.5 km 25 km ahead of the storm. However, Figure 10(a) shows that 20 km ahead of the storm at the later time, the clear-air echo layers were still as high as 1.6 to 1.9 km. This suggests diminished dry subsidence ahead of the storm at this location. Figure 10(a) shows that, within 15 km of the storm, the stable layer rose again but only gently. (At the earlier time, rather stronger ascent had been inferred in Figure 9 by interpolation in the region where echo had not been detectable.) Figure 10(a) also shows a ragged layer just ahead of the storm, centred at a height of 3 km; this is believed to be from the upper boundary of the Flow 4 inflow towards the main updraught before it had been lifted sufficiently to overcome the convective inhibition. Figure 10(b), as with Figure 8(b), shows distorted layers of high spectral width from about 30 to 60 km, associated with the low-level statically stable layer capping the undercurrent beneath the storm. The sharp descent of the layer of highest spectral width from 1.8 km at 43 km to 1.2 km at 48 km is particularly reminiscent of the earlier time. However, the distortion of the low-level flow is revealed even more clearly by the pattern of wind shear and so this will be discussed in more detail shortly.

Another feature of Figure 10(b), more evident than at the earlier time because of the better radar coverage, is the inclined layer of high spectral width sloping down from a height of 6.7 km at 67 km to 3.5 km at 50 km. Comparison with the Doppler RHI in Figure 11(a) shows that this corresponds to the interface between the main slantwise ascent (the blue system-relative rearward flow) and the underlying slantwise descent, i.e. the rear-inflow

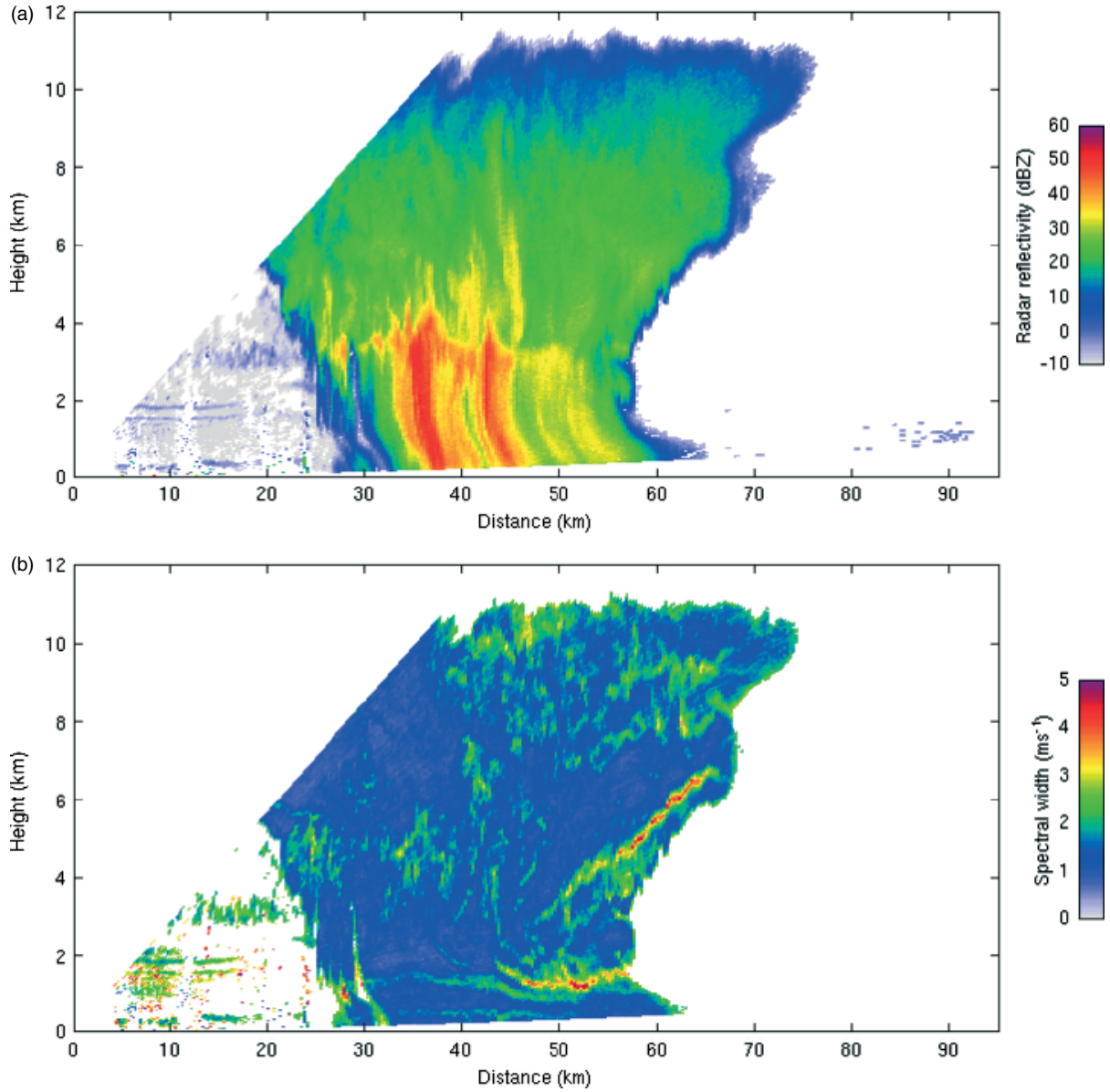

Figure 10. RHI scan from the Chilbolton radar along 232° at 1233 UTC, 24 June 2005: (a) reflectivity (dBz) and (b) spectral width (m s^{-1}). The undercurrent gravity wave was situated between radar ranges 20 and 50 km.

jet (the red and orange system-relative forward flow). Two, more ragged, layers of high spectral width which exist at higher levels (Figure 10(b)), correspond to the upper and lower surfaces of the uppermost layer of slantwise descent (red system-relative forward flow in Figure 11(a)). The midpoint of this flow descends from 9.5 km at 75 km to 7.5 km at 50 km, above the layer of slantwise ascent but below the rearward anvil outflow. High spectral width has previously been observed at the interface between updraught and downdraught by Strauch and Merrem (1976). Also, evidence of sloping layers of high spectral width within an intense thunderstorm has been provided by Archibald *et al.* (1999). They showed that these layers were associated with enhanced eddy dissipation rates at the sheared boundaries of a sloping updraught, particularly at the boundary between sloping up- and downdraughts.

A further interesting feature in Figure 11(a) is the variation in rearward system-relative flow within the cool undercurrent in the lowest kilometre between 20 and 50 km range. Compared with the flow far ahead of the storm (at radar ranges less than 20 km, say), there is a positive anomaly in the magnitude of the rearward storm-relative velocity in the rear part of the storm (deep area of red and yellow beyond 45 km) and a negative anomaly in the front part (a little yellow and orange but no red between between 32 and 42 km). The maximum rearward flow relative to the system increases from 18 to 23 m s^{-1} between 42 and 48 km. This region of divergence is directly beneath the nose of the overrunning rear-inflow jet (red), suggesting a possible cause-and-effect relationship. We have already gained some insight into the nature of this relationship from the local reduction in height of the layers of high spectral width seen in Figure 10(b) and earlier in Figure 8(b). An even clearer indication is provided by the pattern of vertical wind shear derived from the Doppler RHI.

Figure 11(b) shows the component of vertical shear resolved in the plane of the RHI scan. This has been derived by calculating the vertical gradient of the Doppler velocity field shown in Figure 11(a). Like the spectral-width plot in Figure 10(b), it resolves a lot of detailed structure because of

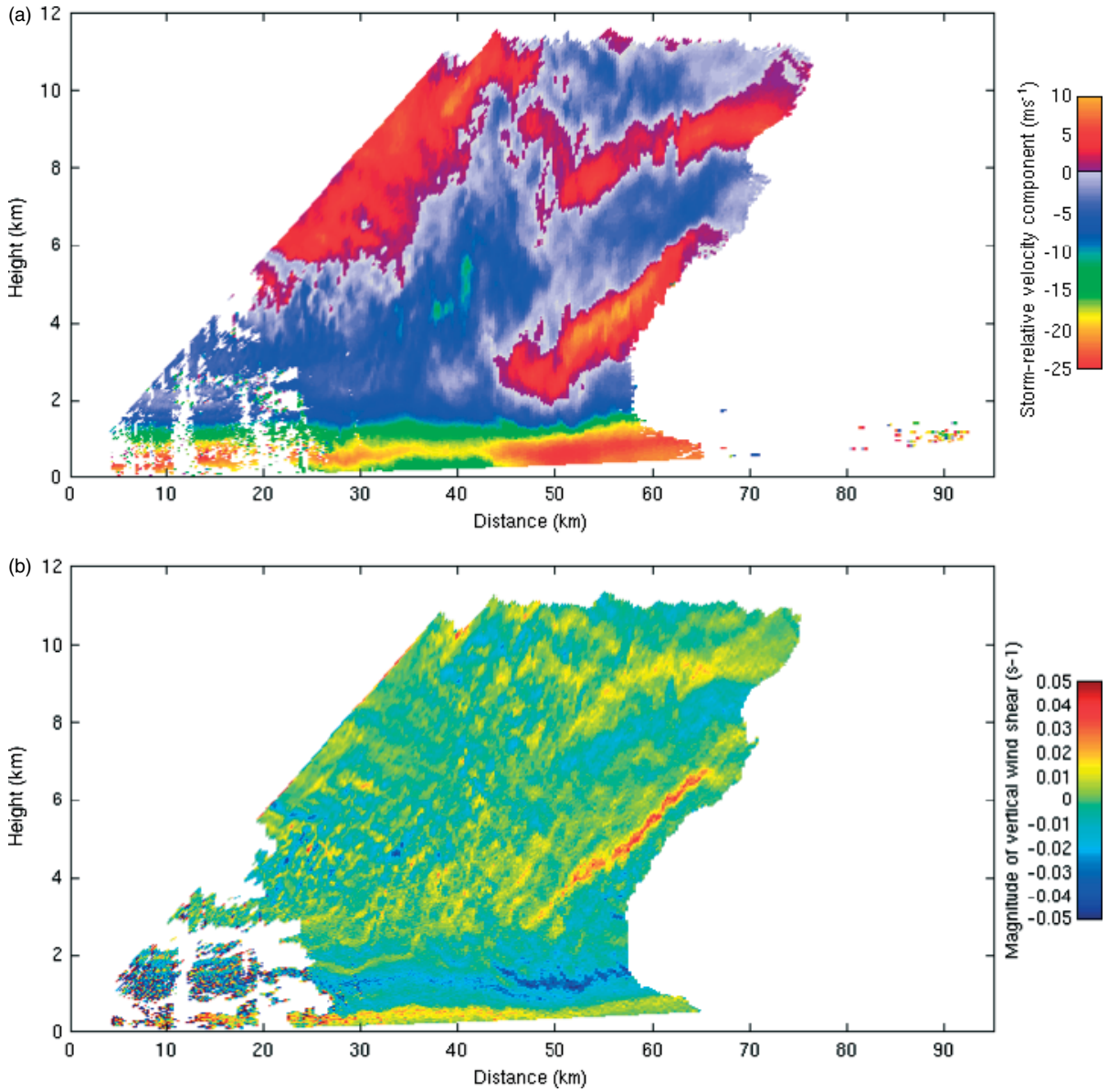

Figure 11. RHI scan as in Figure 10, but showing (a) Doppler velocity ($m\,s^{-1}$) as in Figure 8(c), and (b) line-of-sight component of vertical wind shear derived from (a) (s^{-1}).

the narrowness of the beamwidth of the Chilbolton radar. Although it shows even more detailed structure than the spectral-width plot, one can see patterns that are similar to those in Figure 10(b), which of course is influenced by turbulence as well as wind shear. Three well-defined features of the shear pattern in Figure 11(b) are:

1. the interface between the rearward anvil outflow and the upper layer of slantwise descent (yellow $> 0.1\,s^{-1}$),
2. the interface between the main slantwise ascent and the lowermost layer of slantwise descent, i.e. the rear-inflow jet (orange $> 0.2\,s^{-1}$),
3. the low-level stable layer that descends from 1.8 km at 43 km, beneath the leading edge of the rear-inflow jet, to 1.2 km at 48 km, before rising again beyond 52 km, beneath and behind the impact zone of the rear-inflow jet, (dark blue $> 0.4\,s^{-1}$ and negative).

A particularly informative aspect of Figure 11(b) is the fine structure of the shear in the statically stable layer and undercurrent in the lowest 2 km or so, in the region close to, and ahead of, where the rear-inflow jet impacted upon it. These shear layers (sheets) show up as multiple layers which probably pre-existed before the arrival of the storm but which were then perturbed by processes associated with the passage of the storm. We regard these shear layers as effectively material surfaces which to a first approximation, assuming stationarity, can be interpreted as streamlines. The region where these 'streamlines' descend relatively steeply between 43 and 48 km corresponds to the divergent zone in Figure 11(a) where the system-relative rearward flow in the lowest kilometre accelerated beneath the nose of the overrunning rear-inflow jet. Assuming, to a first approximation, that the flow was essentially two-dimensional, such acceleration is seen to be a consequence of the local constriction of the flow. These, and other principal flows inferred from Figure 11(b), have been traced onto a composite diagram which is discussed next.

Figure 12 shows a synthesis of the information derived from Figures 10 and 11, together with information on anvil extent from the MSG satellite, using a rather similar format

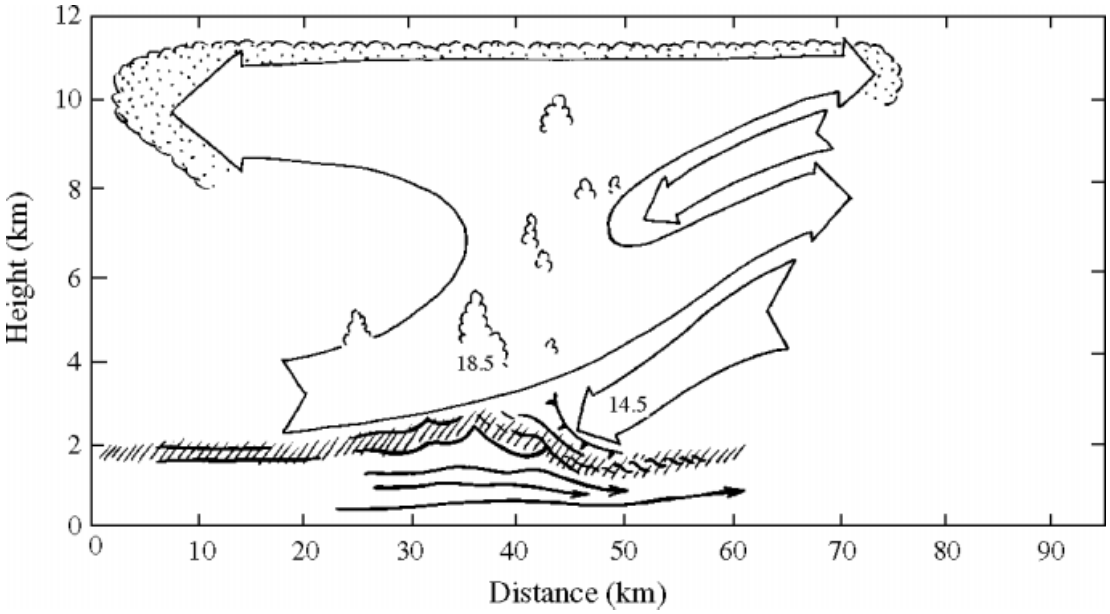

Figure 12. Synthesis broadly as in Figure 9, but for 1233 UTC based on Figures 10 and 11. The synthesis in this diagram is represented more simply than that in Figure 9 insofar as the lower limb of the updraught inflow (Flow 2) is not shown explicitly; instead we have chosen to represent some of the detailed perturbations of the low-level flow. Aloft, the slantwise-flow arrows beyond 50 km radar range are consistent with the velocity anomalies depicted in Figure 11(a) which are associated with slantwise up- and downdraughts separated by layers of high spectral width and shear as shown in Figures 10(b) and 11(b). The lines below 2 km at radar ranges between 5 and 22 km have been derived from the reflectivity layers; beyond 25 km the lines have been derived from the stratification in the wind shear. The lowest three lines are drawn with arrow heads to denote the strong rearward storm-relative motion of the cool undercurrent air close to the ground. The hatched shading associated with some of these lines indicates the inferred statically stable layer at the top of the undercurrent. The spot values, 18.5 and 14.5, indicate local theta-w values in °C, estimated from the height of the radar bright band as explained in the text.

to that in Figure 9. Also shown in Figure 12 are two spot values of theta-w inferred from extreme values in the height of the radar bright band (derived from a plot of linear depolarization ratio, not shown) assuming the bright band corresponds to a local wet-bulb temperature of 0 °C. One of these spot values, 18.5 °C, is seen to have been situated in the main updraught within the lower part of a convective plume as inferred from the mantle-shaped spectral-width signature; this is in line with the maximum theta-w value of 18.3 °C at 2.3 km (770 hPa) seen in the 1100 sounding in the inflow to the storm's convective updraught. The other spot value of theta-w, 14.5 °C, is within the rear-inflow jet; this value is marginally lower than, but not grossly inconsistent with, the lowest theta-w value of 15 °C measured in the layer between about 4 and 6 km in the 1300 Swanage sounding released behind the storm.

A key feature of Figure 12 is the layer denoted by the hatched shading, characterized by strong shear and strong static stability. Although solid arrows like those in Figure 9 are not shown at low levels in Figure 12 (because they would obscure the slightly more detailed streamlines shown here), the layer of hatched shading in Figure 12 appears to be centred on the region between the Flow 1 and Flow 3 arrows in Figure 9. At radar ranges out to 22 km, this feature has been inferred from the reflectivity layering shown in Figure 10(a); beyond 25 km it has been inferred from the distorted layers of strong shear in Figure 11(b). As was seen at the earlier time in Figure 9, the top of this stable layer manifests a raised wave-like structure over a distance of almost 20 km ahead of the nose of the rear-inflow jet. Undulations can be seen within the wave with a horizontal wavelength of 7 km. These form cusps, the crests of which extend upwards to 2.5 km at 36 and 43 km, implying strong vertical mixing in this region.

The low-level streamlines in Figure 12, inferred as already explained from Figure 11(b), represent the rearward system-relative flow of the cool undercurrent air (corresponding to Flow 1 in Figure 9), situated beneath the main layer of strongly stratified air. While not participating directly in the overlying convection or slantwise circulations, this flow, like the strongly stratified layer just above it, would nevertheless have been affected by them, in particular by the impact of the rear-inflow jet. Not only did the depth of the cool air increase in the wave ahead of the nose of the rear-inflow jet, but it also decreased just behind the wave to levels below the original height.

Figure 12 shows that at heights between 1 and 2 km, where the flow in the stable layer behind the wave descended and accelerated, the flow broke up into billows as at the earlier time. According to the radiosonde data in Figure 4, the bulk Richardson number, *Ri*, over the 500 m deep isothermal layer between 1 and 1.5 km was 0.5. In view of the observed local doubling of vertical wind shear (see the transition along a 'streamline', at 43 km range and 1.8 km height, from light blue to dark blue in Figure 11(b)), it is not unreasonable to expect *Ri* to have decreased below the critical value of 0.25 beneath the impacting rear-inflow jet. These billows are therefore attributed to Kelvin – Helmholtz instability.

3.3. RHI scan at 1423 UTC: a time of negligible residual convection but with an extensive rain area sustained by less steeply inclined slantwise circulations

By 1423, when the MCS was scanned receding from the radar, there was very little convection associated with it. This interpretation is supported by the absence of tall columns of high reflectivity (Figure 13(a)) and by the lack of mantle-shaped regions of high spectral width (not shown). However,

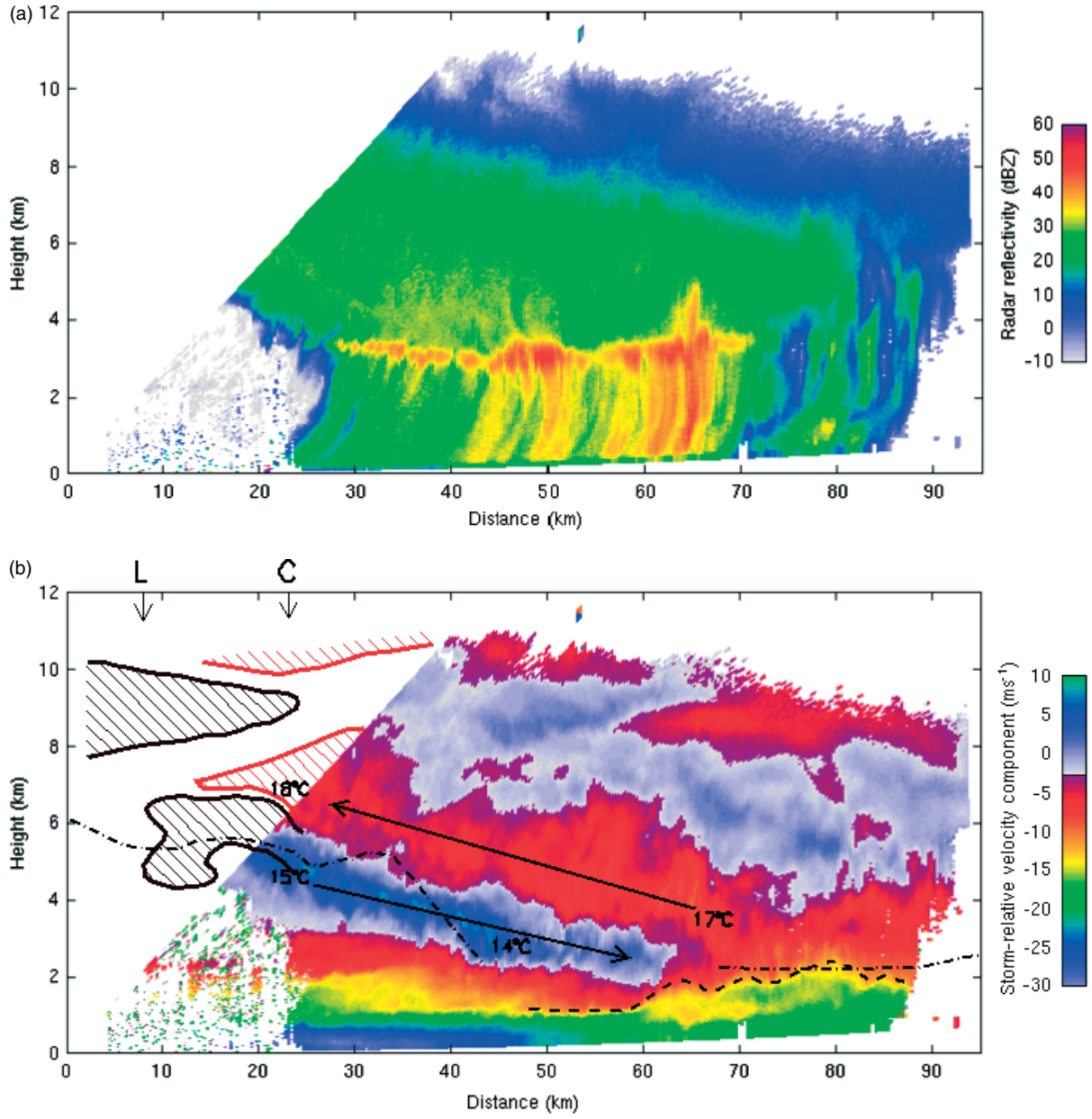

Figure 13. RHI scan from the Chilbolton radar along 044° showing the MCS receding from the radar at 1423 UTC, 24 June 2005: (a) reflectivity (dBz) and (b) Doppler velocity ($m\,s^{-1}$). Positive velocities in (b) are in the direction of travel of the storm, i.e. away from the radar, and the blue and green colours are duplicated, corresponding to positive velocities above 2 km and (large) negative velocities below 2 km. As in Figures 8(c) and 11(a), the colour key is labelled in terms of storm-relative velocities, albeit with the colour sequence reversed such that the rear-inflow jet, for example, is blue (rather than red in the earlier figures when the storm was approaching the radar). To clarify the sense of the storm-relative flows, long arrows are superimposed on the rear-inflow jet and the slantwise ascent above it; as at other times, the rearward relative flow (right to left) is particularly strong in the undercurrent close to the ground. The dashed line denotes the strongly sheared layer at the top of the wave as derived from the Doppler shear plot (not shown). The red and black cross-hatched contours, for ground-relative velocity components of 15 and 20 $m\,s^{-1}$, respectively, are drawn on the basis of data from the Chilbolton (C) and Larkhill (L) radiosondes released at 1400 and 1402, respectively, the storm-relative locations of which are depicted by arrows along the top of (b). The spot values, 17 and 14, in the rearward-directed slantwise updraught and rear-inflow jet, respectively, indicate local theta-w values in °C, estimated from the height of the radar bright band as in Figure 12; the spot values, 18 and 15, in these same flows, were obtained directly from the 1400 Chilbolton radiosonde. Also plotted in (b) (dash-dotted lines) is the cloud base obtained from the CT75K lidar ceilometer at Chilbolton; the lidar was able to penetrate light rain to observe the cloud base but heavier rain prevented detection of the cloud base between 43 and 68 km.

Figure 13(a) shows that, although the precipitation was lighter than before, the extent of stratiform precipitation, and of the associated anvil echo, had grown as a result of the horizontal extension of the slantwise circulations that accompanied the decrease in their slope. At earlier times, when there had been significant convection, MCS C travelled at about 15 $m\,s^{-1}$, but its speed of travel had increased to 18 $m\,s^{-1}$ by the time depicted in Figure 13. Comparison of Figure 13(b) with Figures 9 and 12 shows that there was an increase with time in the horizontal extent of the raised part of the undercurrent associated with the wave (20 km at 1155, 25 km at 1233 and $>$ 27 km at 1423). This indicates that the leading edge of the wave was propagating slightly faster than the nose of the rear-inflow jet.

When interpreting the Doppler data in Figure 13(b), it is necessary to bear in mind that, since the MCS was now travelling away from rather than towards the radar, and since the colour sequence is tied to direction with respect to the radar, the system-relative velocity components then have to be interpreted in terms of a colour bar that is reversed

compared with those in Figures 8(c) and 11(a). Thus the blue colour above 2 km represents system-relative velocities of 0 to 8 m s^{-1} in the main rear-inflow jet (emphasized by the long arrow in Figure 13(b)). The small areas of green within the rear-inflow jet correspond to system-relative velocities of just over 8 m s^{-1}. Although Figure 13(b) shows that the system-relative horizontal velocities of the slantwise flows were still as strong as they were at the earlier times, the vertical velocities are likely to have roughly halved because of the diminution in slope from 1 in 4 to 1 in 9.

Also plotted in Figure 13(b) are the wind components within the plane of the section as derived from two radiosondes launched behind the core of the MCS, just within the rear part of the anvil outflow. One was from Chilbolton at 1400 and the other from Larkhill about 20 km west of Chilbolton, at 1402. The positions of the two soundings relative to the MCS at 1433 are indicated by the arrows, labelled C and L, at the top of the figure. Black and red contours, respectively, are drawn bounding layers where the sondes measured ground-relative wind components of more than 15 m s^{-1} away from the radar (areas hatched in black correspond to light blue and dark blue in the radar-data scheme) and less than 10 m s^{-1} (areas hatched in red, corresponding to the red, as opposed to maroon, radar colour). Notice that a distinct positive velocity anomaly associated with the rear-inflow jet was detected by the Chilbolton sounding, which ascended within the storm's precipitation area, but not by the Larkhill sounding, which was just outside the precipitation but close to the anvil edge. Relative inflow velocities into the rear-inflow jet detected by the Larkhill radiosonde were close to zero, whereas the Doppler data in Figure 13(b) show a few values within the storm that were stronger than 8 m s^{-1} along the axis of this flow. This suggests that the rear-inflow jet, as found by Klimowski (1994), was being generated by the MCS itself at this time. This does not rule out the possibility of a stronger environmental flow feeding the rear-inflow jet and contributing to the development of the MCS at a much earlier time.

The tephigram for the 1400 Chilbolton sounding (not shown) indicated that the layer between 4 and 6 km (620 to 480 hPa), corresponding to the rear-inflow jet, was characterized by unsaturated air with a minimum in theta-w of 15 °C, compared with a maximum of 18 °C in the overlying moist slantwise ascent. These values are plotted at 23 km range in Figure 13(b). The height of the radar bright band reached a minimum in the rear-inflow jet and a maximum in the ascending flow. These heights have been used, as before, to estimate the minimum and maximum values of theta-w, and these are also plotted in Figure 13(b). The resulting value of 14 °C in the rear-inflow jet compares with the 15 °C measured directly by the sonde in another part of the same flow. The value of 17 °C in the ascending flow compares with the 18 °C measured directly.

The dash-dotted lines plotted in Figure 13(b) represent the height of the cloud base as inferred from a time record obtained by the CT75K lidar ceilometer located at Chilbolton. Between ranges of 20 and 40 km, the cloud base was situated close to the interface between the moist slantwise ascending flow and the underlying descending, and hence slightly subsaturated, rear-inflow jet. This is consistent with evaporation of ice playing a significant role in cooling and intensifying the rear-inflow jet (Forbes and Clark, 2003).

The cloud base within the area of heaviest precipitation, though not as high as in much of the rear-inflow jet, was nevertheless still as high as 2.2 km nearby at 68 km range. (The ceilometer was unable to observe cloud base within the heavy precipitation itself.) This indicates the potential for significant cooling by evaporation of rain within the undercurrent, as indicated by the temperature anomalies shown in the AWS plot in Figure 5. As noted earlier, there is no Doppler evidence of the rear-inflow jet or any other downdraught from aloft penetrating to the surface and so the region of divergence within the undercurrent between 45 and 64 km range in Figure 13(b) indicates a shallow downdraught generated mainly within the undercurrent and largely beneath cloud base (for which evaporation of rain is therefore likely to have been important). This is reminiscent of the weak and shallow downdraughts that originated beneath an inversion and from ahead of the storm as observed by Fankhauser *et al.* (1992) and also deduced by Brugge and Moncrieff (1992) in a numerical study.

4. Summary and concluding discussion

In this paper we have presented an observational case-study of a mesoscale convective system using data from CSIP that provides new insight into the relationship between three aspects of the structure: (i) elevated convection, (ii) slantwise circulations and (iii) an associated wave in the cool undercurrent. Details of the wave structure will be addressed in a separate paper, the purpose here being to focus on the slantwise circulations and hence to examine the wave only insofar as its relationship to the overall storm structure is concerned. A more complete understanding of how these different features develop and interact requires a complementary modelling approach and this, too, is left to a later study. Even with these limitations, however, the present analysis still provides considerable insight into the nature of the interaction between the different processes within this important class of storm.

The coexistence of slantwise circulations and upright convection within MCSs is well known (e.g. Fritsch and Forbes, 2001; Johnson and Mapes, 2001; Wakimoto, 2001). In particular, there is a large body of literature on the downdraught component of the slantwise circulation, known as the rear-inflow jet. What is less well known in the case of a so-called Type-1 MCS due to elevated convection above a cool layer is the way in which the slantwise circulation relates to the wave generated at low levels. The fortuitous passage of a MCS directly towards and then away from a sensitive, high-resolution Doppler radar over a 3 h period, combined with special CSIP radiosonde ascents well-placed with respect to the inflow towards the storm, have enabled useful progress to be made towards revealing this relationship. Some of the main findings and inferences relating to this MCS (MCS C) are listed below:

1. Detailed observations of the initiation of MCS C were not made, but satellite and radar-network imagery showed that it formed over the sea off the south coast of England, close to the southern edge of an existing MCS. A nearby radiosonde showed that the MCS was associated with elevated convection derived from air with high theta-w travelling from between the south and southwest above a cool northeasterly flow,

referred to as an undercurrent. Although elevated convection was not observed on any other occasions during the almost 3-month long period of CSIP, it is nevertheless known to be a fairly common occurrence. A similar case of a MCS with elevated convection was observed near southern Britain by Browning and Hill (1984) but elevated convection occurs more frequently in the more continental USA (Wilson and Roberts, 2006). According to Fritsch and Forbes (2001), cool undercurrents characteristic of Type-1 MCSs can be associated with nocturnal cooling of the boundary layer or, as in the present case, with a baroclinic zone.

2. Air with high theta-w destined to feed the convective updraughts, existed in one, and possibly two, separate layer(s) above the cool undercurrent: one was centred at 1.3 km, the other at 2.3 km above ground level. Both of these layers had to be lifted to overcome CIN, the latter by 0.4 km and the former by as much as 1.4 km.
3. There was evidence of compensating dry descent around the storm, which suppressed nearby convection during the early stages, but the predominant downdraughts were within the precipitation area and subject to evaporative cooling. Cool downdraughts occurred at middle levels and, separately, within the undercurrent at low levels. The evidence from the Doppler radar suggested that air in the moist downdraughts above the undercurrent was not able to penetrate the undercurrent to reach the ground. Similar behaviour was observed in the mesoscale convective complexes in the USA studied by Fortune *et al.* (1992), Smull and Augustine (1993) and Trier and Parsons (1993). It was also inferred by Browning and Hill (1984) in the UK on the basis of surface measurements.
4. Vigorous upright convection occupied the layer from 3 to over 10 km during the early period of the storm, but some of the updraught air was unable to penetrate much above a weakly stable layer at 7 km. This may have been why updraught outflows developed at two distinct levels: only the undiluted cores were able to reach the higher level.
5. The outflow of air from the top of the updraughts was towards both the front and rear of the storm in the case of the upper of the two outflows (i.e. anvil spreading in all directions) but was mainly towards the rear in the case of the lower outflow, which exhibited slantwise ascent.
6. Slantwise downdraughts formed beneath both of the two rearward updraught outflows. The lower slantwise downdraught constituted a rear-inflow jet that was moderately strong according to the criterion of Smull and Houze (1987). A similar pair of slantwise downdraughts associated with a MCS has also been observed by Grim and Rauber (2005) in the USA. The interpretation of the data was made more difficult because their Doppler radar did not view the system along its line of approach. Nevertheless, they were able to show that, as in the present case, the two flows entered the rear of the system at around 9 and 5 km, respectively, and that they were laterally extensive. The appearance and multiplicity of the slantwise circulations, as well as their occurrence within a baroclinic zone in the present case, recalls the 'stacked slantwise circulations' analyzed by Browning *et al.* (2001) in association with ana-cold fronts. They attributed the circulations to a combination of delta-M adjustment and CSI. The actual spacing of the two slantwise updraughts in the MCS was, however, greater than in the ana-cold fronts and may instead simply reflect the differing buoyancies of two sets of rising air parcels in the main convection causing them to be detrained at different heights and thereby generate rear inflows at two different heights.
7. The pair of stacked slantwise circulations persisted rather longer than the intense upright convection and accompanying heavy rain. Once the convection had essentially died away, the remaining slantwise circulations adopted a shallower slope (1 in 9 compared with 1 in 4 earlier) and produced stratiform precipitation over an increasingly wide area.
8. The rear-inflow jet was fed by air of relatively low theta-w approaching the rear of the storm at middle levels. The associated storm-relative inflow velocity in the upstream environment was weak, especially during the storm's mature/decaying stage; however, the rear-inflow jet strengthened within the storm itself, indicating the importance of physical processes such as the evaporation of precipitation, especially ice (Forbes and Clark, 2003).
9. The rear-inflow jet descended to the top of the undercurrent. Although it did not penetrate the undercurrent, it strongly perturbed it. Directly beneath the impacting rear-inflow jet, the top of the undercurrent was depressed whilst, ahead of it, the top was elevated in the form of a series of cusped waves (wavelength 7 km). It is inferred that the deepening of parts of the undercurrent gave rise to the lifting of the overlying air of high theta-w, and this lifting was sufficient to overcome the CIN referred to above under item 2.
10. The wave distortion of the undercurrent, whilst probably not a pure bore, did resemble an atmospheric bore in some respects. Bores are common in situations of elevated convection but most studies appear to have been of bores generated by an impulse such as a density current. Once generated, such bores often propagate away from the process generating them. In the present case, however, the wave structure and the impacting rear-inflow jet remained tightly coupled and it is possible that the impacting jet played a role in sustaining it. Alternatively, the wave may be a low-level gravity wave excited by latent heating in the convection, as in the studies of Schumacher and Johnson (2008) and Schumacher (2009), or by diabatic cooling, as in Crook and Moncrieff (1988).
11. The absence of strong winds at the surface within the MCS is consistent with the failure of the rear-inflow jet to reach the ground and produce a strong cold pool. Nevertheless, unlike in a pure atmospheric bore such as observed by Wakimoto and Kingsmill (1995), there was some decrease in surface temperature as the storm passed over. This fall in surface temperature is likely to have been due in part to cloud shadowing (Marsham *et al.*, 2007a, b) and also to evaporation of rain as it fell through the undercurrent. The evaporation together with precipitation loading, will have intensified the shallow downdraughts

forming within part of the undercurrent. Shallow downdraughts within an undercurrent have been identified in a numerical study by Brugge and Moncrieff (1992) and observationally by Fankhauser *et al.* (1992). However, the associated wind and temperature perturbations were not strong or sharp enough to indicate a substantial density current in the present case, nor was the air brought to rest relative to the system. Thus the low-level disturbance could perhaps be regarded not so much as a density current as a gravity wave without stagnation (Crook and Moncrieff, 1988). The nature of the low-level disturbance will be examined in detail in a separate paper.

12. Strong mixing was indicated at the top of the undercurrent directly beneath the impacting rear-inflow jet, being manifested in the form of large-amplitude Kelvin – Helmholtz billows in a region of enhanced shear. Mixing was probably strong also in association with the cusped regions of the elevated wave structure.

This study raises some interesting questions:

- Lafore and Moncrieff (1989) have shown how the rear-inflow jet is related to buoyancy and pressure perturbations which arise from heat sources and sinks due to condensation and evaporation and Pandya and Durran (1996) suggest it is part of a gravity-wave response to the mean diabatic heating in the convection. However, what determines the actual slope of the rear-inflow jet, and in particular, what caused the marked decrease in slope with time in the present case?
- The rear-inflow jet is part of a slantwise circulation but why were there two such circulations in the present case? We have suggested above that one possible reason for the occurrence of two layers of slantwise ascent in the present case may have been the differing buoyancies of two sets of rising air parcels causing them to be detrained from the convective updraught at two different levels. The slantwise descending flows were then generated beneath them. An alternative way of accounting for the multiple layering of the slantwise circulations might be via a gravity-wave generation argument along the lines discussed by Pandya and Durran (1996).
- According to Wakimoto (2001), if a rear-inflow jet descends to the surface, it may increase surface convergence along the gust front. This may strengthen the density current and enhance the system by triggering new convection. Presumably the failure of the rear-inflow jet to penetrate to the surface, as in the present study, impedes the creation of a strong density current. How important would this be to the maintenance or otherwise of an intense MCS, and to what extent therefore do these processes need to be represented within NWP models capable of resolving MCSs?
- It is hypothesised that three factors may contribute to generating the wave observed in the undercurrent: the constriction of the undercurrent by the impacting rear-inflow jet, the diabatic cooling below the MCS (Crook and Moncrieff, 1988) and diabatic heating within the MCS (Schumacher and Johnson, 2008; Schumacher, 2009). What are the relative contributions of these factors and how do they interact? How important, too, is the additional cooling by evaporation of the already cool undercurrent in inhibiting the penetration of the rear-inflow jet to the surface and thereby inhibiting the development of a gravity current and the resulting strong surface winds? Although diabatic cooling within the undercurrent will to some extent diminish the chance of the rear-inflow jet penetrating to the ground, diabatic cooling within the rear-inflow jet itself will of course increase the chance of this happening. Therefore, in modelling the response to these processes, it is important to represent accurately the true depth of the undercurrent.
- Koch *et al.* (2008) have demonstrated the important role that bores accompanying MCSs have in promoting turbulent mixing. The present study shows the top of the cool undercurrent being deformed by long-wavelength cusped undulations and by shorter-wavelength Kelvin – Helmholtz billows, which together are likely to be the principal agents of the mixing in the present study. Does the distortion of the undercurrent by the impacting rear-inflow jet have a controlling influence in sustaining these mixing processes and how important is it to represent this process within NWP models?

Acknowledgements

The original CSIP project and the extended analysis phase leading to the present paper were funded under grants by the Natural Environment Research Council (NERC; NER/O/S/2002 00971 and NE/B505538/1). Special thanks are due to the many who participated in the CSIP field program, in particular Barbara Brooks (University of Leeds), who deployed the AWSs. CSIP exploited instruments available through the UK Universities' Facility for Atmospheric Measurement (UFAM), also funded by NERC. The Chilbolton Observatory, around which the project was based, is owned by the Science and Technology Facilities Council. Satellite data were from Eumetsat. Operational surface analyses and weather-radar network data were provided by the Met Office. Humphrey Lean from the Joint Centre for Mesoscale Meteorology at Reading kindly provided the Unified Model data from which Figure 2 was generated. Trajectories were derived from ECMWF analyses using the British Atmospheric Data Centre trajectory service. Finally we would like to thank two anonymous reviewers and associate editor Peter Clark for their comments, which have improved both the content and clarity of the paper.

References

Archibald E, Chandra M, Meischner P, Hardaker PJ. 1999. Doppler spectrum width as a measure of atmospheric turbulence. In *COST 75 – Advanced weather radar systems*. Collier CG. (ed.) EUR 18567 EN. European Commission: Brussels. 612–624.

Browning KA, Hill FF. 1984. Structure and evolution of a mesoscale convective system near the British Isles. *Q. J. R. Meteorol. Soc.* **110**: 897–913.

Browning KA, Chapman D, Dixon RS. 2001. Stacked slantwise convective circulations. *Q. J. R. Meteorol. Soc.* **127**: 2513–2536.

Browning KA, Blyth AM, Clark PA, Corsmeier U, Morcrette CJ, Agnew JL, Ballard SP, Bamber D, Barthlott C, Bennett LJ, Beswick KM,

Bitter M, Bozier KE, Brooks BJ, Collier CJ, Davies F, Deny B, Dixon MA, Feuerle T, Forbes RM, Gaffard C, Gray MD, Hankers R, Hewison TJ, Kalthoff N, Khodayar S, Kohler M, C Kottmeier SK, Kunz M, Ladd DN, Lean HW, Lenfant J, Li Z, Marsham JH, McGregor J, Mobbs SD, Nicol JC, Norton E, Parker DJ, Perry FM, Ramatschi F, Ricketts HMA, Roberts NM, Russell A, Schulz H, Slack EC, Vaughan G, Waight J, Wareing DP, Watson RJ, Webb AR, Wieser A. 2007. The convective storm initiation project. *Bull. Amer. Meteorol. Soc.* **88**: 1939–1955.

Brugge R, Moncrieff MW. 1992. Multicell stage of the Munich storm of 12 July 1984: A numerical study. *Tellus* **44A**: 339–355.

Crook NA, Moncrieff MW. 1988. The effect of large-scale convergence on the generation and maintenance of deep moist convection. *J. Atmos. Sci.* **45**: 3606–3624.

Fankhauser JC, Barnes GM, LeMone MA. 1992. Structure of a midlatitude squall line formed in strong unidirectional shear. *Mon. Weather Rev.* **120**: 237–260.

Forbes RM, Clark PA. 2003. Sensitivity of extratropical cyclone mesoscale structure to the parametrization of ice microphysical processes. *Q. J. R. Meteorol. Soc.* **129**: 1123–1148.

Fortune MA, Cotton WR, McAnelly RL. 1992. Frontal-wave-like evolution in some mesoscale convective complexes. *Mon. Weather Rev.* **120**: 1279–1300.

Fritsch JM, Forbes GS. 2001. Mesoscale convective systems. In *Severe convective storms. Meteorol. Monograph* **50**: Amer. Meteorol. Soc: Boston, USA. 323–357.

Goddard JFW, Eastment JD, Thurai M. 1994. The Chilbolton Advanced Meteorological Radar: A tool for multidisciplinary atmospheric research. *Electron. Commun. Eng. J.* **6**: 77–86.

Grim JA, Rauber RM. 2005. 'Dual rear inflow jets within the 26 August 2003 derecho'. In *Preprints to 11th AMS Conf. on Mesoscale Processes*, JPJ5.15. Amer. Meteorol. Soc: Boston, USA.

Houze RA. 1993. *Cloud dynamics.* Academic Press: San Diego, USA.

Houze RA. 2004. Mesoscale convective systems. *Rev. Geophys.* **42**: RG4003. DOI: 10.1029/2004RG000150.

Houze RA, Rutledge SA, Biggerstaff MI, Smull BF. 1989. Interpretation of Doppler weather radar displays of midlatitude mesoscale convective systems. *Bull. Amer. Meteorol. Soc.* **70**: 608–619.

Johnson RH, Mapes BE. 2001. Mesoscale processes and severe convective weather. Pp 71–122 in *Severe convective storms. Meteorol. Monograph*, *No. 50*. Amer. Meteorol. Soc: Boston, USA.

Kingsmill DE, Crook NA. 2003. An observational study of atmospheric bore formation from colliding density currents. *Mon. Weather Rev.* **131**: 2985–3002.

Klimowski BA. 1994. Initiation and development of rear inflow within the 28–29 June 1989 North Dakota mesoconvective system. *Mon. Weather Rev.* **122**: 765–779.

Knupp KR. 2006. Observational analysis of a gust front to bore to solitary wave transition within an evolving nocturnal boundary layer. *J. Atmos. Sci.* **63**: 2016–2035.

Koch SE, Feltz W, Fabry F, Pagowski M, Geerts B, Bedka KM, Miller DO, Wilson JW. 2008. Turbulent mixing processes in atmospheric bores and solitary waves deduced from profiling systems and numerical simulation. *Mon. Weather Rev.* **136**: 1373–1400.

Lafore JP, Moncrieff MW. 1989. A numerical investigation of the organization and interaction of the convective and stratiform regions of tropical squall lines. *J. Atmos. Sci.* **46**: 521–544.

Ludlam FH. 1980. *Clouds and storms.* Pennsylvania State Univ. Press: USA.

Maddox RA. 1980. Mesoscale convective complexes. *Bull. Amer. Meteorol. Soc.* **61**: 1374–1387.

Marsham JH, Morcrette CJ, Browning KA, Blyth AM, Parker DJ, Corsmeier U, Kalthoff N, Kohler M. 2007a. Variable cirrus shading during CSIP IOP 5, Part I: Effects on convective initiation. *Q. J. R. Meteorol. Soc.* **133**: 1643–1660.

Marsham JH, Blyth AM, Parker DJ, Beswick K, Browning KA, Corsmeier U, Kalthoff N, Khodayar S, Morcrette CJ, Norton EG. 2007b. Variable cirrus shading during CSIP IOP 5, Part II: Effects on the convective boundary layer. *Q. J. R. Meteorol. Soc.* **133**: 1661–1675.

Pandya RE, Durran DR. 1996. The influence of convectively generated thermal forcing on the mesoscale circulation around squall lines. *J. Atmos. Sci.* **53**: 2924–2951.

Parker MD. 2008. Response of simulated squall lines to low-level cooling. *J. Atmos. Sci.* **65**: 1323–134.

Reynolds DR, Smith AD, Chapman JW. 2008.. A radar study of emigratory flight and layer formation by insects at dawn over southern Britain. *B. Entomol. Res.* **98**: 35–52.

Schumacher RS. 2009. Mechanisms for quasi-stationary behaviour in simulated heavy-rain-producing convective systems. *J. Atmos. Sci.* **66**: 1543–1568.

Schumacher RS, Johnson RH. 2008. Mesoscale processes contributing to extreme rainfall in a midlatitude warm-season flash flood. *Mon. Weather Rev.* **136**: 3964–3986.

Simpson JE. 1997. *Gravity currents in the environment and the laboratory.* Cambridge University Press: Cambridge, UK.

Smull BF, Augustine JA. 1993. Multiscale analysis of a mature mesoscale convective system. *Mon. Weather Rev.* **121**: 103–132.

Smull BF, Houze Jr RA. 1987. Rear inflow in squall lines with trailing stratiform precipitation. *Mon. Weather Rev.* **115**: 2869–2889.

Strauch RG, Merrem FH. 1976. Structure of an evolving hailstorm, Part III: Internal structure from Doppler radar. *Mon. Weather Rev.* **104**: 588–595.

Trier SB, Parsons EB. 1993. Evolution of environmental conditions preceding the development of a nocturnal mesoscale convective complex. *Mon. Weather Rev.* **121**: 1078–1098.

Wakimoto RM. 2001. Convectively driven high wind events. In *Severe convective storms. Meteorol. Monograph* **50**: Amer. Meteorol. Soc: Boston, USA. 255–298.

Wakimoto RM, Kingsmill DE. 1995. Structure of an atmospheric undular bore generated from colliding boundaries during CaPE. *Mon. Weather Rev.* **123**: 1374–1393.

Wilson JW, Roberts RD. 2006. Summary of convective storm initiation and evolution during IHOP: Observational and modeling perspective. *Mon. Weather Rev.* **134**: 23–47.

